Research Paper

Geochemistry and geochronology of mafic rocks from the Spanish Central System: Constraints on the mantle evolution beneath central Spain

D. Orejana [a,*], C. Villaseca [a,b], M. Kristoffersen [c]

[a] Dpto. Mineralogía y Petrología, Facultad de Ciencias Geológicas, Universidad Complutense de Madrid, 28040, Madrid, Spain
[b] Instituto de Geociencias IGEO (UCM, CSIC), 28040, Madrid, Spain
[c] Department of Geosciences, University of Oslo, P.O. Box 1047, Blindern, N-0316, Oslo, Norway

ARTICLE INFO

ABSTRACT

The Spanish Central System (SCS) contains several suites of Palaeozoic mafic igneous intrusions with contrasting geochemical affinity: Ordovician tholeiitic metabasites, Variscan calc-alkaline gabbros (Gb1) and microdiorites (Gb2), shoshonitic monzogabbros (Gb3) and alkaline diabases and lamprophyres (Gb4). Not all of these rocks are accurately dated, and several aspects of their genesis are still poorly understood. We present new whole-rock geochemical data (major and trace elements, and Sr–Nd isotopes), U–Pb and Lu–Hf isotopic ratios on magmatic zircons and $^{40}Ar/^{39}Ar$ amphibole geochronology results in order to establish a precise chronology for the successive events of magmatism in the SCS, and discuss the nature of their mantle sources. Accurate ages have been determined for the Variscan gabbros (305–294 Ma), the microdiorites (299 Ma) and the accompanying felsic porphyries (292 Ma), the shoshonitic monzogabbros (285 Ma), and the alkaline diabases (274 Ma) and mon-zosyenites (271–264 Ma). According to this information, the Variscan mafic magmatism would be mainly concentrated in the range of 305–294 Ma, with a final manifestation represented by the minor shoshonitic dykes. The alkaline magmatism proved to be slightly older than previously thought and yielded at least two distinct pulses: diabases and lamprophyres–monzosyenites. Zircon Hf isotopes evidence the involvement of depleted and slightly enriched mantle sources. The bulk of the εHf values are in the broad range of −8 to +11, indicative of melting both depleted and enriched mantle regions. The high within-sample Hf isotope variation (up to ~11 epsilon units) shown by samples from the Variscan series (gabbros, microdiorites and monzogabbros) could be explained mainly by hybridisation of magmas derived from heterogeneous lithospheric mantle sources. Pressure estimates indicate that the Variscan mafic magmas were extracted from the lithosphere. The Nd–Hf isotopic composition of these suites of rocks suggests the recycling of pelitic sediments during the Cadomian orogeny. Deeper (asthenospheric) mantle levels were involved in the generation of the alkaline suite, whose anomalous negative εHf values (moderately decoupled with respect to radiogenic Nd) could be associated with subducted oceanic components raised by mantle upwelling associated with lithosphere thinning and extension during the Permian.

1. Introduction

The study of primitive mafic rocks is an indirect way to determine the composition of their mantle sources. The analysis of different isotopic systems (e.g., Sr, Nd, Pb, Hf, O, C isotopic ratios), as well as the whole-rock trace element composition, have been demonstrated as powerful tools to unravel complicated histories of mantle evolution (enrichment and depletion processes), and to determine the possible involvement of different mantle or crustal components in shallow mafic magmatism

(e.g., Chauvel et al., 2008; Zhao et al., 2009; Tappe et al., 2013).

In recent years, zircon has been extensively used to characterise the nature of mantle sources because: (i) it is a robust mineral capable of resisting metamorphic, igneous and sedimentary cycles, (ii) it may crystallise from crustal and mantle-derived melts, (iii) it contains significant isotopic information (U–Pb, Lu–Hf, O) and, (iv) microanalytical techniques allow the age of formation and isotopic signatures from the same zircon area to be determined. Studies of mafic rocks which combine whole-rock geochemical data with the zircon isotopic composition have

---

been used to discuss the type of crustal components recycled into the mantle, the origin of deep-seated metasomatic agents and the lithospheric vs. asthenospheric nature of the magma sources (Griffin et al., 2000; Nowell et al., 2004; Chen et al., 2008; Cheong et al., 2015). When several magmatic suites of contrasting composition are placed within an accurate temporal context, this kind of data can also provide a perspective on how the mantle composition has evolved over time and what changes can be ascribed to certain geodynamic settings (e.g., Tappe et al., 2007, 2016; Dai et al., 2011; Zhang et al., 2012; Couzinié et al., 2016; Gardiner et al., 2016).

The Palaeozoic mafic rocks from the Spanish Central System (SCS) are mostly sills, dykes and small gabbroic intrusions, which represent mantle-melting events produced over an approximate age interval of 210 Myr, in at least three different stages: pre-Variscan (Early to Late Ordovician: 475–450 Ma), syn- to late-Variscan (Late Carboniferous–Early Permian: 310–285 Ma) or clearly post-Variscan (Middle Permian: 271–264 Ma) times. Their variable geochemical affinity testifies to the existence of heterogeneous mantle sources and/or the involvement of distinct processes that might have modified the mantle composition over time. Although much research have been done on the geochemistry and geochronology of these rocks (e.g., Villaseca et al., 2004, 2011, 2015; Scarrow et al., 2006, 2009, 2011; Orejana et al., 2008, 2009, 2017), the age of some of these magmatic events are still uncertain and several genetic aspects are poorly constrained, such as the number and nature of the metasomatic agents involved in the mantle sources and the role played by crustal components. Our study contributes whole-rock data, zircon U–Pb and Lu–Hf isotopic signatures and Ar–Ar geochronology, with the aim of improving the scarce data of some poorly sampled magmatic groups of mafic dykes, accurately dating magmatic events of unclear age and discussing the nature of the mantle sources on the basis of a comprehensive zircon Lu–Hf isotopic dataset.

The Spanish Central System (SCS) mafic magmatic events have been assigned to distinct geotectonic frameworks: oceanic rifting (pre-Variscan tholeiites), continental collision (Variscan calc-alkaline suites) and post-collisional extension prior to the onset of the break-up of Pangea (post-Variscan alkaline rocks), which would allow different processes of crust–mantle interaction and metasomatism. The study of the SCS mantle-derived rocks, which intruded over a long period of time and show contrasting geochemical affinities, can thus help to characterise the main changes in the lithospheric mantle during the Palaeozoic in connection with likely tectonomagmatic events.

2. Geological setting

The Spanish Central System is a mountain range exposing a large Variscan granitic batholith and its country metamorphic rocks. It is part of the Central-Iberian Zone, which represents the innermost region of the Variscan Iberian Belt (Fig. 1). The metamorphic rocks consist of: (i) metasedimentary sequences deposited in a back-arc basin during the Cadomian orogenic cycle (Neoproterozoic–Cambrian) and in the context of a later continental passive margin (Ordovician–Devonian), and ii) Cambrian–Ordovician peraluminous metagranitic orthogneisses dated mostly to 481–496 Ma (U–Pb in zircon; Villaseca et al., 2016).

The magmatic events recorded in the SCS might be ascribed to five main stages: (1) the Cadomian orogeny (e.g., Villaseca et al., 2016), (2) the Ordovician rifting leading to the opening of the Rheic ocean (e.g., Villaseca et al., 2015; Orejana et al., 2017), (3) the collisional Variscan cycle (e.g., Villaseca et al., 1998; Bea et al., 1999; Orejana et al., 2009; Scarrow et al., 2009), (4) the Permian extension (e.g., Orejana et al., 2008; Scarrow et al., 2011), and (5) the Triassic–Jurassic rifting leading to the opening of the Atlantic Ocean (e.g., Cebriá et al., 2003). The last four stages include the intrusion of plutonic or subvolcanic mantle-derived rocks, whose main petrographic and geochemical characteristics are summarised in Table 1.

The first manifestation of mafic magmatism in the SCS corresponds to small dykes, sills or laccoliths intruding into granitic Cambrian–Early
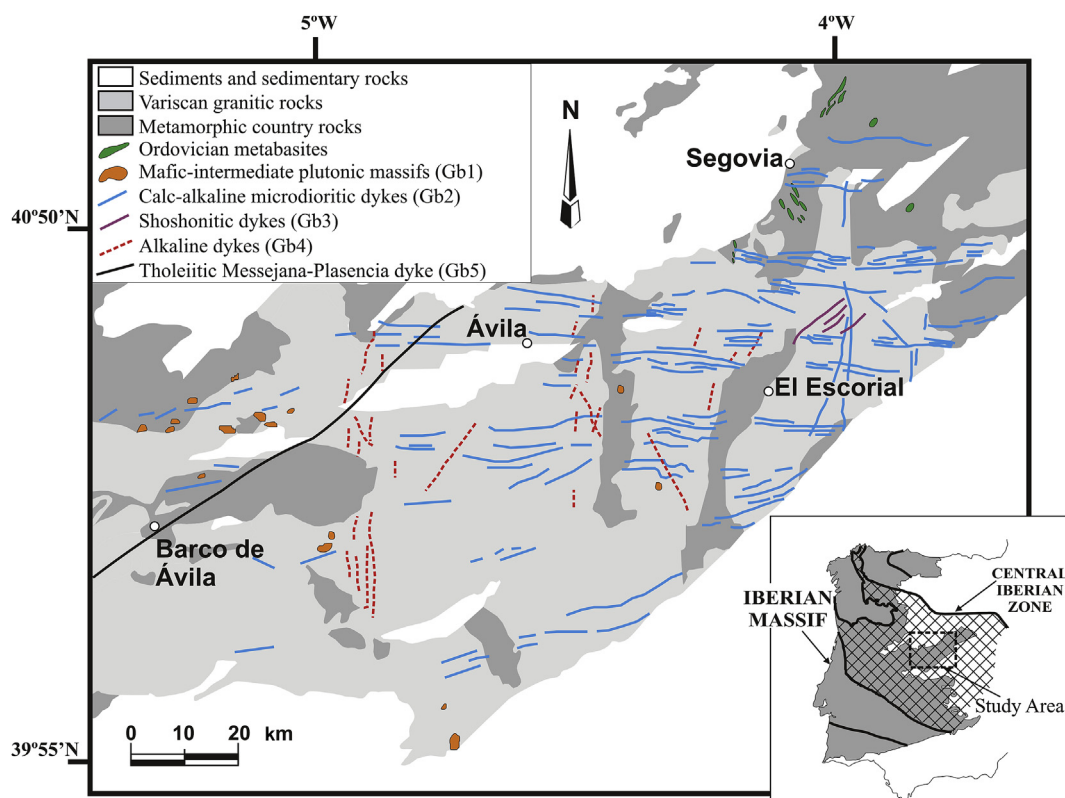

Fig. 1. Geological sketch map of the Spanish Central System showing the location of the outcropping mafic rocks. Nomenclature Gb1 to Gb5 after Villaseca et al. (2004).

Table 1
Main features of the Ordovician to Permian mantle-derived rocks from the Spanish Central System.

Rock group and age[a]	Outcrop	Petrography	Geochemistry	T_{DM} (Nd)[b]
Alkaline dykes (Gb4) (252–274 Ma)	N–S dykes (<2.5 m in thickness). Two groups: (1) Diabases and (2) ultramafic lamprophyres to intermediate to felsic monzo-syenitic porphyries	Mafic to ultramafic terms: camptonitic lamprophyres and diabases. Intermediate to felsic terms: monzonites-syenites. The mafic dykes include Amph, Cpx and Plg megacrysts and deep-seated mafic cumulates.	Strongly alkaline suite. Strong LILE, LREE and HFSE enrichment (Nb–Ta positive anomaly). Bimodal Sr–Nd isotopic composition: moderately depleted (ƐNd = 4–7.1; diabases) and slightly enriched (ƐNd = 1.4 to −1.4; lamprophyres and mono-syenites).	Isotopically depleted: 452–614 (511) Ma; Isotopically enriched: 840–1126 (1021) Ma
Monzonitic dykes (Gb3) (285 Ma)	Scarce and localised NE–SW dykes (0.5–1.5 m in thickness). Some interaction with felsic magmas is occasionally observed.	Microgabbros–Monzogabbros	Subalkaline calc-alkaline suite (shoshonitic). LILE, LREE and Pb enrichment, and Nb–Ta depletion. Enriched Sr–Nd isotopic composition (ƐNd = −1.9 to −3.6).	1129–1191 (1157) Ma
Microdioritic dykes (Gb2) (292–299 Ma)	Abundant mainly W–E dykes (0.5–15 m in thickness). Associated with a widespread suite of felsic dykes (porphyries of rhyolitic to dacitic composition).	Micrograbbbros, microdiorites and Q-microdiorites	Subalkaline calc-alkaline suite (medium-K). LILE, LREE and Pb enrichment, and Nb–Ta depletion. Enriched Sr–Nd isotopic composition (ƐNd = −2.2 to −4.1).	1553–1804 (1668) Ma
Variscan Gabbros (Gb1)(294–305 Ma)	Small rounded plutonic bodies intrusive within post-tectonic granites and associated metamorphic rocks. Mingling/mixing structures (between mafic and felsic magmas) may be observed in the intrusions boundaries.	Olivine gabbros to Q-diorites. Tonalites and granodiorites may appear associated to mixing with felsic magmas. Primary amphibole and phlogopite may be present in all lithologies.	Subalkaline calc-alkaline suite (medium- to high-K). Moderate LILE–LREE and strong Pb enrichment, and Nb–Ta depletion. Slightly depleted to slightly enriched Sr–Nd isotopic composition (ƐNd = 2.4 to −4.4).	1145–1737 (1366) Ma
Metabasites (453–473 Ma)	Small intrusions (sill-type) or boudines in augen gneisses or interbedded within a metasedimentary sequence.	Revenga sector: Olivine meta-gabbros and meta-diorites with igneous textures, and amphibolites. Tenzuela sector: Garnet melamphibolites and leucoamphibolites in massifs subjected to HT–HP metamorphism.	Subalkaline tholeiitic suite. Moderate LILE and LREE enrichment. Nb–Ta negative anomaly. Bimodal Sr–Nd isotopic composition: moderately depleted (ƐNd = 4.3–6) and slightly enriched (ƐNd = 1.5 to −2.7).	Isotopically depleted: 1195–1223 (1209) Ma; Isotopically enriched: 1355–2115 (1684) Ma

[a] The age data have been taken from Perini et al. (2004), Fernández–Suárez et al. (2006), Scarrow et al. (2006), Perini and Timmerman (2008) and this study (alkaline dykes), Galindo et al. (1994) and this study (microdiorites and monzonites), Villaseca et al. (2011) and this study (Gb1 gabbros), Villaseca et al. (2015) and Orejana et al. (2017) (metabasites).

[b] Nd model ages are expressed as ranges, with the average value in brackets. Data calculated for samples with $^{147}Sm/^{144}Nd$ < 0.167 (after criteria of Stern, 2002), using isotopic ratios taken from Bea et al. (1999), Orejana et al. (2008), Scarrow et al. (2011) and this study (alkaline dykes); Villaseca et al. (2004) and this study (microdiorites and monzonites); Orejana et al. (2009) (Gb1 gabbros), Villaseca et al. (2015) and Orejana et al. (2017) (metabasites).

Ordovician augen gneisses or Neoproterozoic–Cambrian metasediments (Fig. 1). These are mainly gabbroic and dioritic metabasites, although more differentiated types (tonalitic) are also present in the Tenzuela massif (Villaseca et al., 2015; Orejana et al., 2017). Two groups of metabasites can be distinguished according to their geochemical and petrographic features (Table 1): those from the Tenzuela sector, and those from the Revenga–El Caloco area. The first group displays a *HP–MT* (eclogite/HP granulite) metamorphic mineral paragenesis due to deep burial during the Variscan collision (Barbero and Villaseca, 2000), whereas primary igneous mineralogy and textures are better preserved in the Revenga area. As a whole, these metabasites constitute tholeiitic series extending from basic to intermediate types. They have been dated to 453–473 Ma (U–Pb zircon geochronology) and the involvement of two different mantle sources has been suggested on the basis of their heterogeneous Sr–Nd isotopic composition (Orejana et al., 2017).

The late stages of the Variscan collision involved the generation of multiple granitic bodies from central to NW Spain. Although scarce, coeval mantle-derived magmas accompanied the felsic melts, giving rise to small gabbro and diorite intrusions (Gb1 in Fig. 1) and km-sized dyke swarms (Fig. 1). U–Pb zircon data of the SCS gabbros imply intrusion ages in the main range of 305–300 Ma (Villaseca et al., 2011, and references therein), in accordance with the ages determined on the SCS granites (e.g., Orejana et al., 2012). Microdioritic dyke swarms, accompanied by felsic granitic porphyries, crosscut the whole SCS batholith (Gb2 in Fig. 1). A poorly constrained age of 296 ± 3 Ma (Rb–Sr

whole-rock isochron; Galindo et al., 1994) has been suggested for these intrusions. The microdiorites are members of a calc-alkaline series, similar to the plutonic gabbroic-dioritic Gb1 association, with fractionation and magma mixing as the main differentiation processes involved (Huertas and Villaseca, 1994; Orejana et al., 2009; Scarrow et al., 2009). The last magmatic event of the Variscan cycle is represented by monzonitic microgabbroic dykes of shoshonitic affinity and uncertain age, which outcrop within a restricted area of the SCS (Gb3 swarm in Fig. 1). These Variscan mafic rocks (gabbros, microdiorites and monzonitic gabbros) all have incompatible trace element contents (e.g., negative Nb–Ta anomalies, high Th/Yb, low Ce/Pb) characteristic of magmas from active continental margins or collisional orogens (Table 1). A lithospheric mantle has been proposed as the source of their primary melts, with a significant contribution from crustal recycling (e.g., Villaseca et al., 2004; Orejana et al., 2009).

A suite of volatile-rich mafic-ultramafic alkaline dykes follows the calc-alkaline series. This group may be subdivided into (i) diabases, and (ii) lamprophyres to monzosyenitic porphyries on the basis of petrographic and geochemical data (Orejana et al., 2008) (Table 1). Previous geochronological studies have provided Permian intrusion ages in the range of 252–264 Ma (Ar–Ar in amphibole and U–Pb in zircon; Perini et al., 2004; Fernández–Suárez et al., 2006; Scarrow et al., 2006; Perini and Timmerman, 2008), although only lamprophyres (or the associated syenitic porphyries) were sampled. Their Sr–Nd isotopic ratios suggest the melting of lithospheric and asthenospheric mantle sources previously

metasomatised by deep-seated K-volatile-rich melts (Orejana et al., 2008).

In this study we will follow the nomenclature used by Villaseca et al. (2004) to distinguish the Variscan and post-Variscan suites of mafic rocks: Gabbros (Gb1), microdioritic dykes (Gb2), shoshonitic monzogabbros (Gb3) and the alkaline suite (Gb4). A fifth suite (Gb5) corresponding to the large tholeiitic Messejana–Plasencia dyke was also included in the work of Villaseca et al. (2004), however, these latter mafic rocks have not provided magmatic zircons and their age of intrusion (in the Jurassic–Triassic transition) has already been accurately determined (203 ± 2 Ma; Ar–Ar in biotite; Dunn et al., 1998), so they do not fit the objectives of our study.

3. Analytical methods

3.1. Whole-rock composition and isotopic (Rb–Sr, Sm–Nd) ratios

Major and trace element analyses were carried out at ACTLABS (Ancaster, Ontario, Canada). The samples were melted using $LiBO_2$ and dissolved with HNO_3. Inductively coupled plasma atomic emission spectrometry (ICP–AES) was used for major element analysis, and trace elements were determined by inductively coupled plasma mass spectrometry (ICP–MS). Uncertainties in major elements range from 1% to 3%, except for MnO (5%–10%). The precision of ICP–MS analyses at low concentration levels has been evaluated from the repeated analyses of the international standards NIST-694, DNC-1, JR-1, W-2, SY-4 and BIR-1. The precision for trace elements is in the range 1%–5%. More information on the procedure, precision and accuracy of ICP–MS analyses can be provided by Actlabs upon request. Whole-rock chemical data ($n = 9$) is presented in Supplementary Table 1.

Sr–Nd whole-rock isotopic analyses were carried out at the CAI de Geocronología y Geoquímica Isotópica (Complutense University of Madrid), using an automated VG Sector 54 multicollector thermal ionisation mass spectrometer. Analytical data was acquired in multidynamic mode. The analytical procedures used in this laboratory have been described elsewhere (Reyes et al., 1997). Repeated analyses of NBS 987 gave $^{87}Sr/^{86}Sr = 0.710246 \pm 11$ (2σ, $n = 8$) and the values of $^{143}Nd/^{144}Nd = 0.511856 \pm 11$ (2σ, $n = 6$) were obtained for the JM Nd standard. The 2σ analytical errors are 0.01% for $^{87}Sr/^{86}Sr$ and 0.006% for $^{143}Nd/^{144}Nd$, which yield a 2σ error on εNd calculation of ±0.1. Nd model ages have been calculated for the analysed data and those taken from the literature (Table 1), considering the following ratios for the depleted mantle: $^{147}Sm/^{144}Nd = 0.2137$ and $^{143}Nd/^{144}Nd = 0.51315$. Whole-rock Sr–Nd isotope results are listed in Supplementary Table 2.

3.2. U–Pb and Lu–Hf isotopic ratios in zircon

Zircons were separated using standard techniques and a representative selection was handpicked from each sample. These grains were mounted in epoxy resin for microanalytical analysis at the IBERSIM laboratories (University of Granada, Spain), together with the reference zircons TEMORA 1, SL13 and REG. The mount was polished and the zircon central portions were imaged with transmitted and reflected light, and with cathodoluminescence on a scanning electron microscope. Selected areas in the grains of four samples (80317, 80324, 112905 and 116452) were analysed for U, Th and Pb isotopes on the Sensitive High Resolution Ion Microprobe (SHRIMP II) with each analysis consisting of six scans through the relevant mass range. The primary beam, composed of $^{16}O^{16}O^+$, was set to an intensity of about 5 nA, with a 120 μm Kohler aperture, which generates 17 μm × 20 μm elliptical spots on the target. All calibration procedures were performed on the standards included on the same mount. One TEMORA zircon standard was analysed for every four unknown analyses. Data was reduced using the SHRIMPTOOLS software (available from www.ugr.es/~fbea), specifically developed for IBERSIMS by Fernando Bea. More details can be found in http://www.ugr.es/~ibersims/ibersims/Sample_analysis_and_methods

.html. Pb/U ratios were normalised relative to a value of 0.06683 for the $^{206}Pb/^{238}U$ ratio of the TEMORA reference zircon, equivalent to an age of 417 ± 1 Ma (IDTIMS in zircon; Black et al., 2003). Concentration data was normalised against zircon standard SL13 (210 ppm U, Black et al., 2004).

U–Pb age determinations on three gabbroic samples (T149, T150 and T151) were performed by laser ablation ICP-MS at the GEMOC, at the Macquarie University of Sydney, using a New Wave 213 laser ablation microprobe, attached to an Agilent 7500 quadrupole ICP-MS. The laser system delivers a beam of 213-nm UV light from a frequency-quintupled Nd: YAG laser. Analyses were carried out with a beam diameter of 30 μm, a 5 Hz repetition rate and energies of 60–100 mJ/pulse. Typical ablation times are 100–120 s, resulting in pits 30–40 μm deep. The time-resolved signals were processed using GLITTER interactive software. The standards used were the 91500 zircon (1064 ± 2.5 Ma; Wiedenbeck et al., 1995) and the Mud Tank zircon (734 ± 32 Ma; Black and Gulson, 1978), with the GEMOCGJ-1 standard as a quality control (608.5 Ma). Their measured mean values are within 2σ of the recommended values. Uncertainties given for individual analyses (ratios and ages) are at the 1σ level; however, uncertainties in the calculated concordia ages are reported as 95% confidence limits. Concordia plots were drawn using Isoplot 3.0 software (Ludwig, 2003). All ages are 204-corrected $^{206}Pb/^{238}U$ ages (Supplementary Table 3).

The Lu–Hf zircon isotope ratios were determined by LA-MC-ICPMS in two different laboratories. Eight samples (80317, 80324, 110406, 110407, 110410, 112905, 114793 and 114796) were analysed at the Department of Geosciences (University of Oslo) using a Nu Plasma HR mass spectrometer and a Cetac LSX-213 G2+ laser microprobe. Masses 172 to 179 were measured simultaneously in Faraday collectors, using the Nu Plasma collector block. Laser-ablation conditions were: 50 μm static spot (aperture imaging mode), 5 Hz pulse frequency and ca. 2 J/cm² beam fluence. Each ablation was preceded by a 30 s on-mass background measurement. The total Hf signal obtained was in the range 1.5–4.0 V. Under these conditions, 120–150 s of ablation are required to obtain an internal precision of $\leq \pm0.000020$ (1σ). Isotope ratios were calculated using the Nu Plasma time-resolved analysis software. The raw data was corrected for mass discrimination using an exponential law, the mass discrimination factor for Hf (fHf) was determined assuming $^{179}Hf/^{177}Hf = 0.7325$ (Patchett and Tatsumoto, 1980). The Mud Tank and LV-11 reference standards were used for analysis calibration. Their analysed mean values: 0.282497 ± 0.000037 (2σ; $n = 200$), and 0.282830 ± 0.000068 (2σ; $n = 119$), respectively, agree with the mean published values: 0.282507 ± 0.000006 for MT (Woodhead and Hergt, 2005) and 0.282830 ± 0.000028 for LV-11 (Heinonen et al., 2010). The protocol used for correction for interference from ^{176}Lu, ^{176}Yb and corrected ^{176}Hf is given in Elburg et al. (2013).

The remaining Hf isotope analyses (samples T149, T150 and T151) were performed in situ using a 213 nm Nd:YAG laser microprobe attached to a Nu Plasma multi-collector ICP-MS system at the GEMOC laboratories. Each analysis was carried out with a beam diameter of 40–55 μm, a 5 Hz repetition rate, 60% power output and a beam fluence of about 2 J/cm². The ablation times were 100–200 s, resulting in pits 30–40 μm deep. Griffin et al. (2000, 2004) described the methodology in detail. We repeatedly analysed two zircon standards: 91500 and Mud Tank (MT) to evaluate the accuracy and precision of the laser-ablation results. These reference zircons gave $^{176}Hf/^{177}Hf = 0.282310 \pm 0.000049$ (2σ) and 0.282502 ± 0.000044 (2σ), respectively, which are indistinguishable from other LA-ICP-MS reported values (0.282307 ± 0.000058 for 91500 and 0.282523 ± 0.000043 for MT; Griffin et al., 2006, 2007). The 2σ uncertainty on a single analysis of $^{176}Lu/^{177}Hf$ is ±(0.001%–0.002%) (about 1 epsilon unit), reflecting both analytical uncertainties and the spatial variation of Lu–Hf across many zircons.

The ^{176}Lu decay constant value of 1.865×10^{-11} a^{-1} was used in all calculations (Scherer et al., 2001). Chondritic $^{176}Hf/^{177}Hf = 0.282785$ and $^{176}Lu/^{177}Hf = 0.0336$ (Bouvier et al., 2008) were used to calculate εHf values.

3.3. Ar–Ar geochronology

Two samples were dated by the $^{40}Ar/^{39}Ar$ incremental heating method, corresponding to an amphibole concentrate of a calc-alkaline microdiorite dyke (112900) and a kaersutite megacryst from an alkaline diabase dyke (Supplementary Table 5). Amphiboles were crushed and sieved to obtain a size fraction of 300–600 μm. Further details on sample procedures can be found in Duncan and Keller (2004). Samples were loaded in evacuated quartz tubes together with Fish Canyon sanidine monitor standard (28.201 ± 0.023 Ma; Kuiper et al., 2008) and irradiated in the Oregon State University TRIGA reactor ICIT facility. Analyses were performed at the Argon Geochronology Laboratory of the Oregon State University, using an ARGUS VI multi-collector mass spectrometer equipped with a 25 W Synrad CO_2 laser. Corrections of interferences with Ca and K are given in Wijbrans et al. (1995). The ^4K decay constant used is 5.53×10^{-10} a^{-1} (Min et al., 2000).

Incremental heating plateau ages were calculated using the ArArCALC v2.5.2 software from Koppers (2002). The uncertainties in the apparent ages at each step, as well as the weighted mean plateau ages, are given at the 2σ level.

4. Whole-rock geochemistry of mafic series from central Spain

A detailed discussion of the whole-rock geochemistry of the different suites of basic igneous rocks from central Spain is beyond the scope of this work. An abundant geochemical dataset of these intrusions can be found in the literature, mainly for the Ordovician metabasites, the Variscan gabbros (Gb1) and the alkaline series (Gb4) (Bea et al., 1999; Barbero and Villaseca, 2000; Orejana et al., 2006, 2008, 2009, 2017; Scarrow et al., 2009, 2011; Villaseca et al., 2015), together with a comprehensive interpretation of their genesis. Conversely, little data is available on the Variscan microdiorites (Gb2) and monzogabbros (Gb3) (Huertas, 1990; Huertas and Villaseca, 1994; Villaseca et al., 2004). We have thus analysed nine new samples (5 microdiorites, 3 monzogabbros and 1 alkaline diabase) to complement this latter dataset. The major and trace element contents and the isotopic composition (Sr–Nd) can be found in Supplementary Tables 1 and 2, respectively. The data description (as well as that shown in Figs. 2–4) accounts for all the mafic rocks, including the new analyses and those from the literature.

Most of the mafic igneous series are subalkaline, with the exception of the Permian Gb4 alkaline suite (Fig. 2A). The evolution shown by the
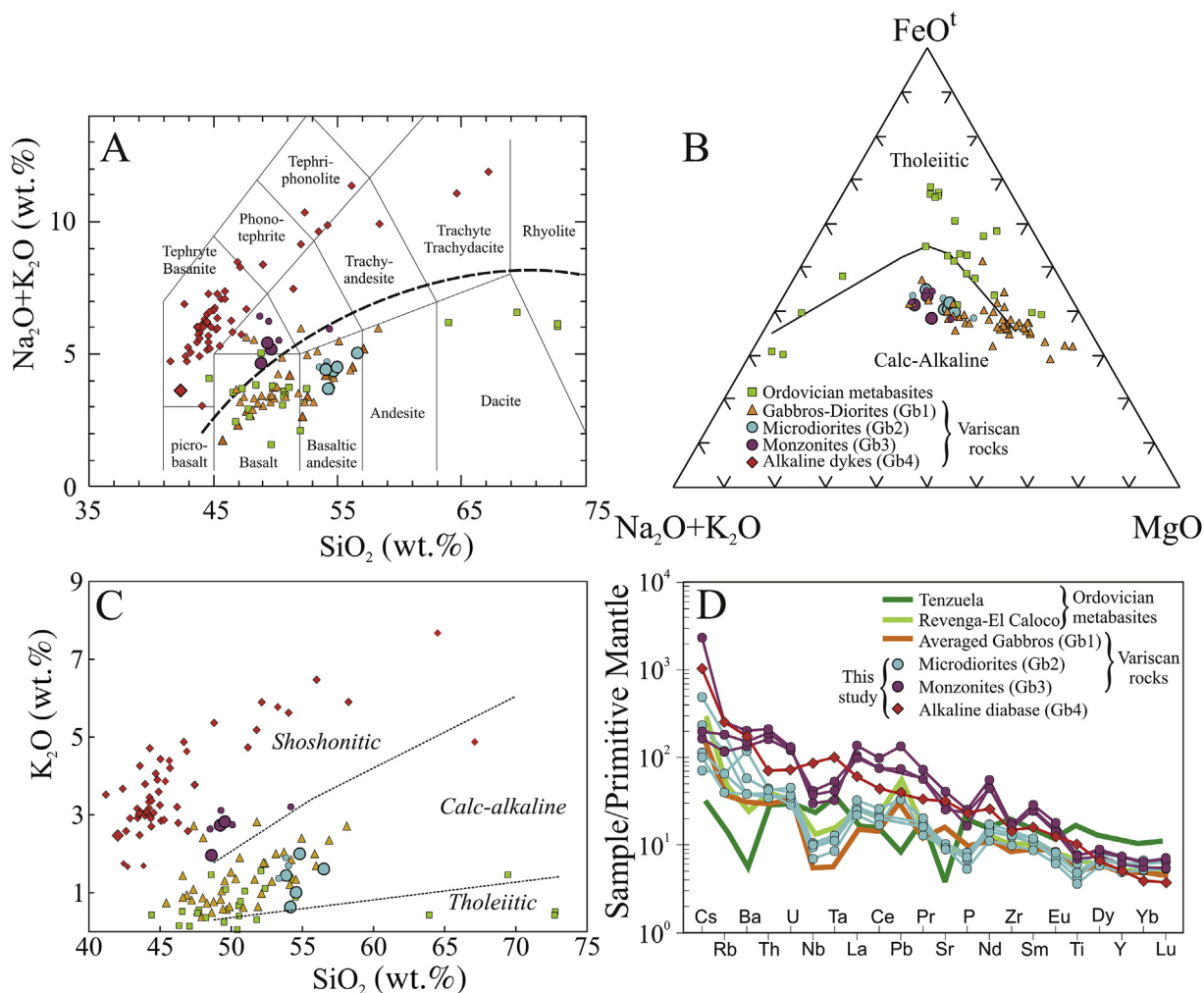
Fig. 2. Whole-rock major (in wt.%) and trace element (in ppm) composition of the mantle-derived rocks from the Spanish Central System: (A) total alkalies vs. SiO_2, (B) AFM diagram, (C) K_2O vs. SiO_2 and (D) primitive mantle-normalised trace element composition of the analysed samples. The larger symbols in diagrams A, B and C represent samples analysed for this study. Smaller symbols are data from the literature: Barbero and Villaseca (2000), Villaseca et al. (2015) and Orejana et al. (2017) for the Ordovician metabasites; Orejana et al. (2009) and Scarrow et al. (2009) for the Gb1 calc-alkaline suite; Villaseca et al. (2004) for the microdioritic and monzonitic dykes (Gb2 and Gb3); and Bea et al. (1999), Orejana et al. (2008) and Scarrow et al. (2011) for the alkaline dykes (Gb4). The average trace element composition of Ordovician metabasites and Gb1 gabbros in Diagram C are representative of the basic terms in those series. Primitive mantle values after McDonough and Sun (1995).

subalkaline series in the AFM diagram (Fig. 2B) allows the distinction of the Ordovician tholeiitic metabasites from the rest of sub-alkaline Variscan mafic rocks (Gb1, Gb2 and Gb3). The metabasites, Gb1 calc-alkaline intrusions and alkaline dykes display a heterogeneous composition, with SiO_2 broadly ranging from 41–45 wt.% to 66–73 wt.% (Fig. 2A). The most primitive samples in these three groups show Mg# values and Cr and Ni concentrations representative of near-primary magmas. Evolution towards the most differentiated types has been related to AFC (fractional crystallisation + assimilation) processes in the case of the metabasites and the alkaline dykes (Orejana et al., 2008, 2009, 2017), whereas the association of the Gb1 gabbros with Q-diorites, tonalities and granodiorites has been explained by mixing and mingling with the abundant Variscan granitic magmas (Orejana et al., 2009; Scarrow et al., 2009; Villaseca et al., 2011). The new analysed samples are similar in composition to the previous Gb2 and Gb3 data and configure two restricted fields without an apparent trend of evolution (Fig. 2A). Intermediate lithologies between the microdiorites (Gb2) or monzonitic gabbros (Gb3) and the accompanying prevalent granitic porphyries have been described in central Spain (Huertas and Villaseca, 1994), however, indicating that the mixing of mantle- and crustal-derived magmas is also possible in these cases. While the Gb2 suite seems to be part of a typical calc-alkaline evolution trend, the Gb3 gabbros stand out for their high K_2O content, indicative of a shoshonitic composition (Supplementary Table 1; Fig. 2C).

Fig. 2D shows the Primitive Mantle-normalised trace element contents of the analysed samples. This data is representative of the bulk Gb2, Gb3 and Gb4 groups (see results in Villaseca et al., 2004 and Orejana et al., 2008). For the sake of clarity, only averaged compositions have been plotted for the metabasites (depleted Tenzuela and enriched Revenga–El Caloco samples) and Gb1 gabbros. A moderate enrichment of LILE and LREE is apparent in the Revenga–El Caloco metabasites, Variscan gabbros and microdioritic dykes. The shoshonitic Gb3 dykes and the alkaline suite show even higher concentrations for these elements (Fig. 2D), and more fractionated chondrite-normalised HREE patterns (Fig. 3B). The trace element composition of the alkaline lamprophyres and diabases closely resembles that of OIB, with HFSE enrichment, Nb–Ta positive anomalies and high Ta/Yb ratios, typical of rocks derived from an enriched mantle reservoir (Figs. 2D and 3A). Moderate to strong Nb–Ta negative anomalies are characteristic in the rest of the mafic suites, excluding the Tenzuela metabasites (Figs. 2D and 3B). The Th/Yb and Ta/Yb ratios of the calc-alkaline and shoshonitic series fall within the field of igneous rocks associated with active continental margins, whereas the metabasites are intermediate between this pole and the mantle array (Fig. 3A).

Overall, the isotopic data extends from a depleted near-MORB composition ($\varepsilon Nd = 7.1$) to a moderately enriched pole ($^{87}Sr/^{86}Sr = 0.708802$) (Fig. 4A). This range is mostly confined to the Mantle Array, excepting a few metabasites (with $\varepsilon Nd > 2$) interpreted as affected by metamorphism (Orejana et al., 2017). The Gb1 gabbros–diorites, metabasites and Gb4 alkaline dykes exhibit a large heterogeneity, although the latter two groups show a bimodal composition (compositional gap between $\varepsilon Nd = 4$–1.5) rather than a continuum. The calc-alkaline mafic dykes are more homogeneous and represent the most radiogenic values (Fig. 4A). This dataset overlaps the composition of mantle xenolith from central and western Europe (Beccaluva et al., 2004 and references therein), including those from central Spain (Villaseca et al., 2010), and its most enriched pole coincides with the isotopic ratios determined for other Variscan gabbroic rocks from nearby regions (Fig. 4A).

The Nd model ages (T_{DM}) calculated for these mafic suites represent a relatively long period of time (2115–452 Ma; Table 1). Samples with high $^{147}Sm/^{144}Nd$ ratios (>0.167) have not been plotted in the diagrams as they may yield unreliable model ages (Stern, 2002). The alkaline dykes provide Nd model ages younger than the other samples, which can be divided in two groups: 452–614 Ma (isotopically depleted diabases) and 840–1126 Ma (isotopically enriched lamprophyres). The rest of the mafic suites demonstrate overlapping T_{DM} ages ranging from 1133 Ma to 2115
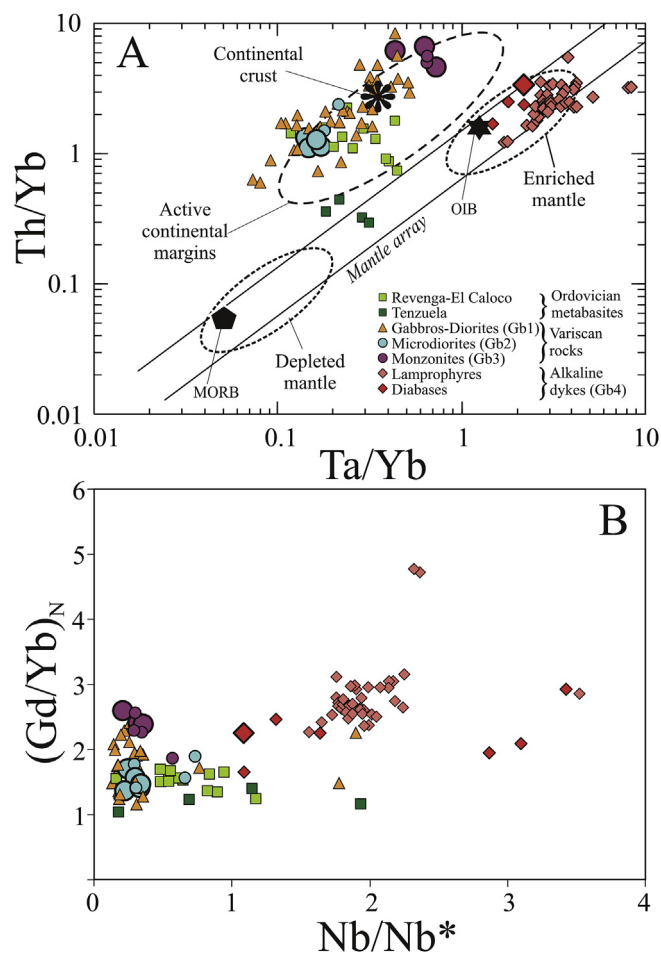

Fig. 3. Incompatible trace element ratios of SCS mantle-derived rocks. (A) Th/Yb vs. Ta/Yb; and (B) Chondrite-normalised Gd/Yb vs. Nb anomaly [Nb/Nb* = $Nb_N/((La_N+U_N)/2)$]. Chondrite values, MORB and OIB average composition in diagram A are taken from Sun and McDonough (1989). Continental crust average composition is taken from Rudnick and Gao (2003). The field of active continental margins after Wilson (1989). Smaller symbols are data from the literature (see references in caption to Fig. 2).

Ma (Fig. 4B). Within this range, the shoshonitic monzogabbros yield younger model ages (mostly < 1190 Ma), whereas metabasites, microdiorites and Variscan gabbros overlap each other in a wider time span (1145–2115 Ma). It is also worth noting that the Ordovician metabasites can be divided into two groups: those from the Tenzuela sector, with lower model ages (1195–1223 Ma), and those from Revenga–El Caloco (1355–2115 Ma).

5. Zircon geochronology

Zircon size, morphology and texture was studied from all samples using transmitted and reflected light microscopy, as well as BSE and CL imaging. The studied zircons are colourless to slightly yellowish, and usually range from 50 to 250 μm in size, although some grains may reach lengths up to 500 μm (Fig. 5). They may be anhedral, mostly because the original crystals are fragmented, but there is a tendency to develop euhedral and subhedral habits, mainly bipyramidal morphologies with aspect ratios commonly from 1:2 to 1:3. The predominant internal structure is oscillatory zoning, followed by unzoned grains. Sector zoning is occasional and the development of bright rims and recrystallisation textures is restricted to the moderately to strongly metamorphosed Ordovician metabasites (Fig. 5).

A total of 143 crystals were analysed for U–Pb isotopes, resulting in
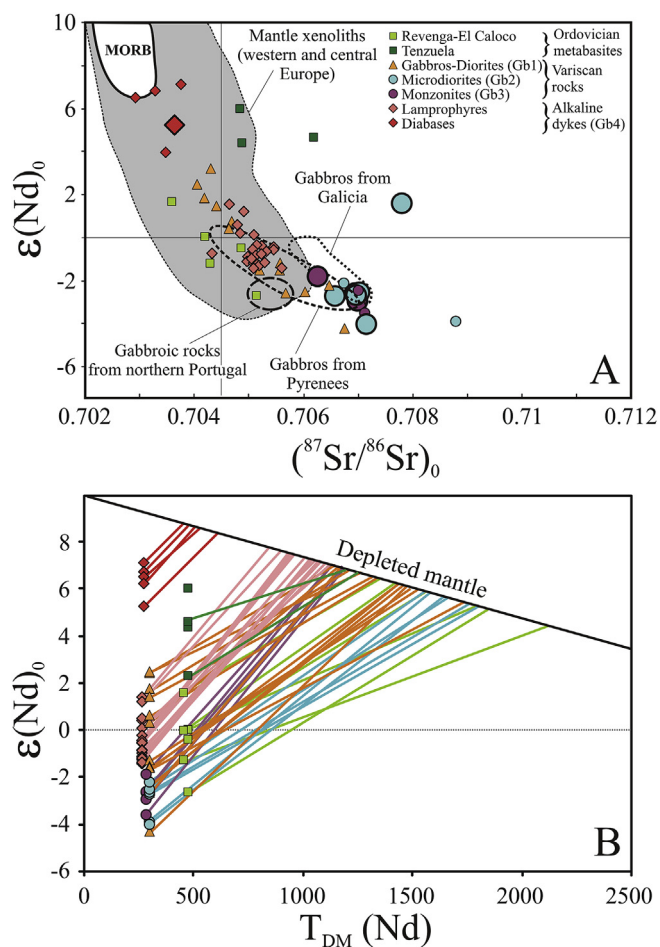
Fig. 4. Initial Sr–Nd isotopic composition (A) and εNd vs. T_{DM} (Nd) (B) of mantle-derived rocks from the Spanish Central System. The larger symbols in Diagram A represent samples analysed for this study. Smaller symbols are data from the literature: Villaseca et al. (2015) and Orejana et al. (2017) for the metabasites; Orejana et al. (2009) for the Gb1 calc-alkaline suite; Villaseca et al. (2004) for the microdioritic and monzonitic dykes; and Bea et al. (1999), Orejana et al. (2008) and Scarrow et al. (2011) for the alkaline dykes. The composition of different Variscan and post-Variscan mafic intrusions from other regions of the Iberian Massif is also plotted for comparison: gabbros from Galicia (Galán et al., 1996), gabbroic rocks from northern Portugal (Dias and Leterrier, 1994; Dias et al., 2002); and gabbros from Pyrenees (Vilá et al., 2005), together with that of mantle xenoliths from western and central Europe (Beccaluva et al., 2004, and references therein). MORB field taken from Wilson (1989).

145 analyses, in samples T149 (*n* = 12), T150 (*n* = 25), T151 (*n* = 22), 116452 (*n* = 20), 80317 (*n* = 20), 80324 (*n* = 20) and 112905 (*n* = 26) (Supplementary Table 3). Discordant analyses (d > 13%) and data showing high common Pb (>1.1%) was not considered for age calculations (21 points) and the resulting 124 data points were plotted in weighted averaged and Wetherill concordia diagrams (Figs. 6 and 7).

5.1. Alkaline dykes (Gb4; samples 80317 and 80324)

Twelve and fifteen analyses from two monzosyenitic alkaline dykes (samples 80317 and 80324) provided $^{206}Pb/^{238}U$ ages in the following ranges: 252–289 Ma and 257–281 Ma (Supplementary Table 3), respectively. The weighted average age calculated for sample 80317 (265.4 ± 4.1 Ma) is slightly younger than that of sample 80324 (271.0 ± 2.1 Ma) (Fig. 6), although they overlap if the associated error is considered. Alternatively, a very similar concordia age has been obtained for sample 80317 (264.7 ± 4.4 Ma). The 13 analyses used to calculate the weighted average age in sample 80324 do not allow a concordia age to be

calculated (Fig. 6). This data perfectly matches the previous results on the same alkaline suite (~264 Ma based mainly on amphibole Ar–Ar geochronology in mafic rocks: Perini et al., 2004; Scarrow et al., 2006; Perini and Timmerman, 2008), although they were determined exclusively on the mafic to ultramafic lamprophyric dykes. The only attempt previously made to date the accompanying alkaline monzosyenitic suite was that by Fernández–Suárez et al. (2006), which provided an age of 252 ± 3.0 Ma based on a small number of zircon spots.

5.2. Shoshonitic dyke (Gb3; sample 112905)

This sample shows a range of $^{206}Pb/^{238}U$ ages from 277 Ma to 295 Ma (Supplementary Table 3). Twenty four zircon analyses were used to calculate a weighted average age of 285 ± 1.4 Ma (Fig. 6). These spots do not yield a concordia age, but the intercept age (287 ± 1.9 Ma) is similar to the above weighted average. The data of 285 Ma can be considered a good approximation to the age of crystallisation for this mafic rock.

5.3. Granite porphyry dyke (sample 116452)

Due to the absence of magmatic zircons in the calc-alkaline microdiorite dykes (Gb2), we sampled the accompanying felsic terms in order to obtain U–Pb zircon ages. The abundant granite porphyry dykes outcropping in the Spanish Central System show complex interactions with the associated microdioritic magma (mingling and mixing features in diverse composite dykes), which demonstrates that they constitute a coeval bimodal magmatism (e.g., Huertas and Villaseca, 1994). An attempt to date the mafic dykes based on Ar–Ar geochronology is presented below.

Zircon analyses from sample 116452 yielded a wide temporal range from 260 Ma to 308 Ma, with the exception of one inheritance (532 ± 7 Ma; Supplementary Table 3). After data filtering, very similar concordia and weighted average ages (291.6 ± 2.5 Ma and 292.1 ± 1.8 Ma, respectively) were calculated (Fig. 6). This data is in agreement with previous results (Rb–Sr whole-rock isochron, 296 ± 3 Ma; Galindo et al., 1994).

5.4. Variscan gabbros (Gb1; samples T149, T150 and T151)

The three analysed gabbros provided ages (after filtering of data) close to the Carboniferous–Permian boundary (Supplementary Table 3). Samples T149 and T151 show a relatively narrow range of $^{206}Pb/^{238}U$ ages, with weighted averages of 294.4 ± 2.7 Ma and 300.8 ± 1.8 Ma, respectively (no concordia ages could be calculated). These results closely resemble the intercept ages (Fig. 7). On the other hand, gabbro T150 displays a broader age spectrum (282–313 Ma) which does not allow an *a priori* straightforward interpretation. This heterogeneous and continuous dataset might be due to Pb loss, but there are no significant differences in the CL internal structure of zircons in this sample (they are mostly unzoned and unaltered), so it is not possible to make an initial selection on the basis of their texture. We have thus applied the TuffZirc method (Ludwig and Mundil, 2002), which is based on slight positive and negative age biases in the dataset and extracts a median age from the largest cluster of ages. The calculated age is 305.0 (+2/–3) Ma, and is similar to the intercept age obtained for the same analyses (Fig. 7). The above results can be considered the best approximation to the crystallisation ages, and they are mostly coincident with previous geochronological data on the SCS Variscan gabbros (300–305 Ma; U–Pb in zircon; Villaseca et al., 2011). However, it is noteworthy that the age calculated for sample T149 (294.4 ± 2.7 Ma) falls out of the above range and represents the youngest age recorded in these gabbroic intrusions.

6. Lu–Hf isotope composition

Lu–Hf isotope ratios were determined in the same spot that U–Pb zircon data was obtained, or within the same zone, resulting in a total of
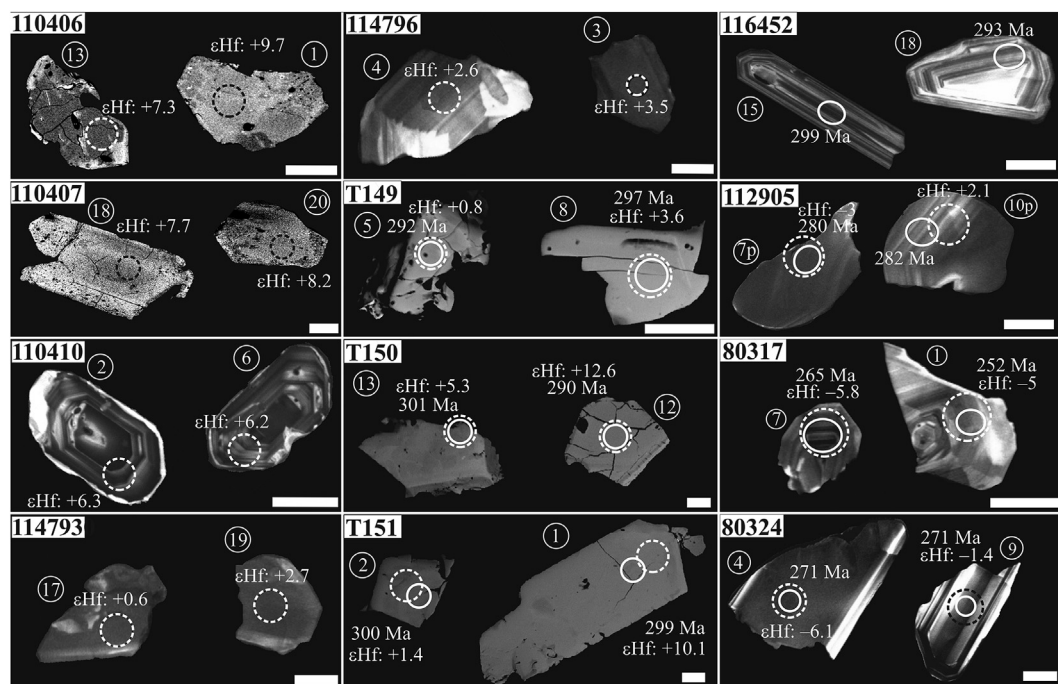
Fig. 5. Cathodoluminescence images of representative zircon grains from Ordovician metabasites (110406, 110407, 110410 from the Tenzuela massif; 114793 from the Revenga area, and 114796 from El Caloco area), Variscan gabbros (T149, T150 and T151), a granite porphyry associated with Gb2 microdiorites (116452), a Gb3 monzogabbro (112905), and monzosyenitic dykes of the Gb4 suite (80317, 80324). Solid-line circles represent U–Pb spots, whereas dashed-line circles indicate the Hf spot. The corresponding age and εHf data for each zircon grain are also shown. The white bar in all images represents 50 μm.

164 analyses in samples T149 ($n = 10$), T150 ($n = 10$), T151 ($n = 10$), 80317 ($n = 16$), 80324 ($n = 12$), 112905 ($n = 23$), 110406 ($n = 12$), 110407 ($n = 20$), 110410 ($n = 18$), 114793 ($n = 16$) and 114796 ($n = 17$) (Supplementary Table 4). Initial zircon Hf isotopic ratios were calculated using the mean ^{206}Pb/^{238}U age obtained for the corresponding intrusion (estimated age of crystallisation). U–Pb zircon ages of the Ordovician metabasites 110406, 110407, 110410, 114793 and 114796 were previously determined by Villaseca et al. (2015) and Orejana et al. (2017). Analyses showing ^{176}Lu/^{177}Hf > 0.005 and high ^{176}Yb/^{177}Hf coupled to high ^{176}Hf/^{177}Hf ratios were rejected because of the potential for uncorrected isobaric interferences. The measured ^{176}Hf/^{177}Hf composition, and the εHf values calculated to the age of crystallisation, are plotted in Fig. 8. The whole dataset is characterised by a pronounce heterogeneity (Supplementary Table 4), with most analyses restricted to values above those of the BSE (εHf > 0) (Fig. 8B).

The alkaline dykes show a slightly enriched zircon Hf isotopic composition, with εHf values ranging from −1.1 to −7.7 (Supplementary Table 4; Fig. 8B). This data is relatively homogeneous and coincident in both samples. The shoshonitic dyke has a similar composition, although with a wider range and slightly higher ratios (Fig. 8A). The Variscan gabbros exhibit the most scattered values, mainly with positive εHf (up to +7), and within-sample variations up to 11 *epsilon* units (Fig. 8B). The wide ranges shown by these samples overlap, and are also equivalent to previous results from other gabbroic intrusions (Villaseca et al., 2011) (Fig. 8B).

The Ordovician metabasites provided consistent data, all plotting above the CHUR (Fig. 8A). Samples 110406 and 110410 give rise to a clear dispersion of ages towards values lower than the estimated age of intrusion. This scattering is probably associated with the Variscan metamorphism, which might lead to Pb loss, while the Lu–Hf system remained undisturbed (e.g., Amelin et al., 2000). Due to the low ^{176}Lu/^{177}Hf ratios of zircon (~0.001–0.003) the ^{176}Hf/^{177}Hf ratios calculated at the age of crystallisation are almost identical to those calculated to the observed age, as evidenced by metabasites 110406 and 110410 (Fig. 8A).

The εHf of the SCS mafic rocks shows a broad positive correlation with the whole-rock εNd values (Fig. 8B), also manifested in a general overlapping of most samples with the *mantle array*. Exceptions to this are the alkaline dykes, which plot below the mantle evolution line, and the most enriched metabasites (114793 and 114796), which plot slightly above (Fig. 8B). The gabbro T115 also falls out of this trend (far below the mantle array) and show a more enriched composition with respect to the other gabbros (εHf < −3.5) (Fig. 8B). The metabasites suite involves two different mantle sources: an isotopically depleted component represented by samples 110406 and 110407 (Tenzuela sector), and an enriched pole defined by samples 114793 and 114796 (Revenga–El Caloco sector) (see Orejana et al., 2017). Sample 110410, which has intermediate isotopic values, has been related to a process of crustal assimilation. No correlation is apparent in the case of the Variscan gabbros, in part due to the large dispersion of the dataset (Fig. 8B).

7. Ar–Ar geochronology

Samples from Gb2 microdiorite and Gb4 diabase dykes did not provide magmatic zircons, so the Ar–Ar method of dating was applied to amphibole separated from two samples: hornblende-rich segregates in microdiorite 112900 and a kaersutite megacryst from an alkaline diabase (Bernuy Salinero dyke; Orejana et al., 2008).

A plateau age of 299.9 ± 1.4 Ma was obtained for microdiorite 112900, based on 27 step ages (Supplementary Table 5; Fig. 9). This age is similar to the inverse isochron age (302.9 ± 2.9 Ma) within error, and could be taken as the most probable age of intrusion of this microdiorite dyke. The SCS microdiorites belong to a bimodal suite of mafic to felsic dyke swarms with W–E strike directions, very abundant in central Spain (e.g., Huertas and Villaseca, 1994), which crosscut granitic plutons dated in the broad age range of 305–297 Ma in the Guadarrama sector (Orejana et al., 2012). The only available age on the felsic dykes (granitic porphyries) from the SCS (296 ± 3 Ma; Rb–Sr isochron in Galindo et al., 1994) overlaps the U–Pb zircon age calculated for sample 116452 (granitic porphyry) in this study (292.1 ± 1.8 Ma).
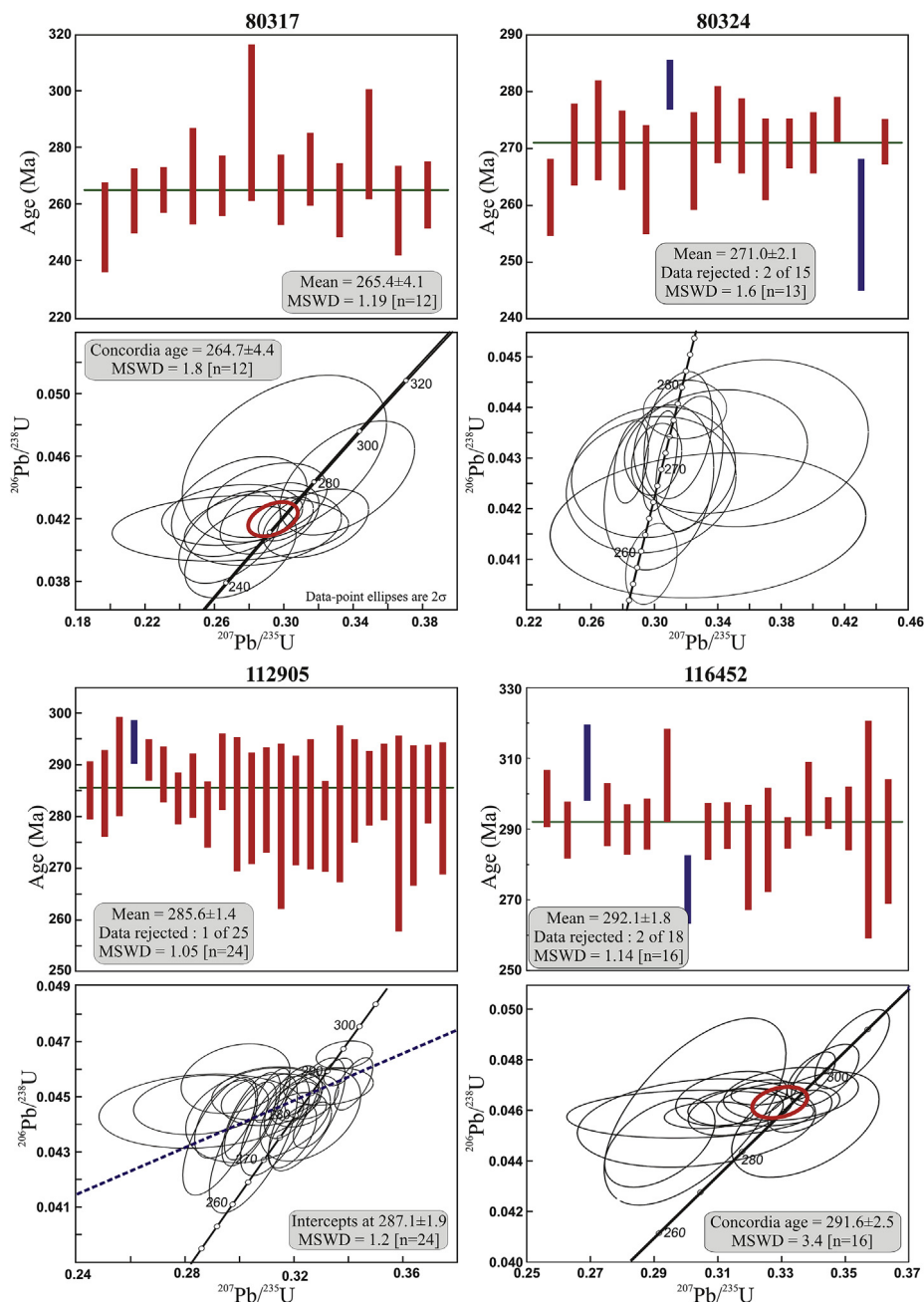
Fig. 6. Weighted average and concordia diagrams showing the SHRIMP U–Pb data for zircons from samples 80317 and 80324 (alkaline dykes), 112905 (shoshonitic dyke) and 116452 (granite porphyry). Error ellipses and error bars are given at the 2σ level. Blue bars are rejected analyses.

The kaersutite megacryst from an alkaline diabase dyke has provided a well constrained age of 274.4 ± 1.5 Ma (plateau age based on 35 steps and 78.9% ^{39}Ar), almost identical to the 274.4 ± 1.7 Ma inverse isochron age (Fig. 9). This age is older than the main age range of the Permian SCS lamprophyres (256–264 Ma; see references in Table 1) and the associated alkaline monzosyenitic samples 80317 and 80324 (264–271 Ma; this study).

8. Discussion

8.1. Geochronological constraints

There have been several events of mafic magmatism in the SCS from Lower Ordovician to Jurassic. Accurate dating of these intrusions has been attempted in recent years, leading to an improvement of the age and

geodynamic constraints (e.g., Dunn et al., 1998; Scarrow et al., 2006; Villaseca et al., 2011, 2015; Orejana et al., 2017). The metabasites outcropping in the Tenzuela, El Caloco and Revenga sectors are the oldest mafic rocks in the SCS (473–453 Ma) and are considered the first manifestation of proto-rifting (Rheic ocean opening) within the Central Iberian Zone (Orejana et al., 2017). A long time span followed this Ordovician event until other mantle-derived magmas intruded into the SCS during the Variscan collisional orogeny. They correspond to small gabbroic-dioritic bodies, which have provided ages within a narrow period (307–300 Ma; U–Pb in zircon; Bea et al., 2006; Zeck et al., 2007; Villaseca et al., 2011). Different suites of mafic dyke swarms with contrasting geochemical affinities (calc-alkaline, shoshonitic, alkaline and tholeiitic) then intruded in the SCS (e.g., Villaseca et al., 2004). Although crosscutting relationships among these dyke groups allowed a likely sequence of emplacement to be identified, precise ages were lacking for
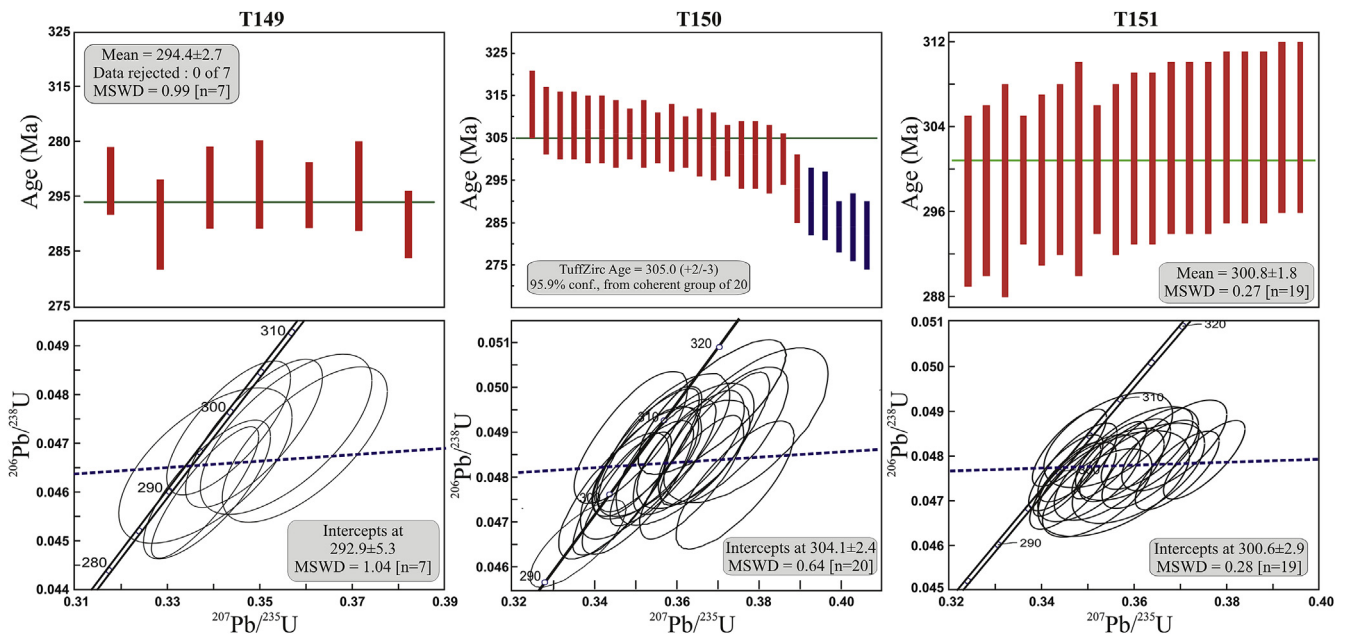
Fig. 7. Weighted average and concordia diagrams showing the SHRIMP U–Pb data for zircons from samples T149, T150 and T151 (Variscan Gb1 gabbros). Error ellipses are given at the 2σ level. Blue bars are rejected analyses.
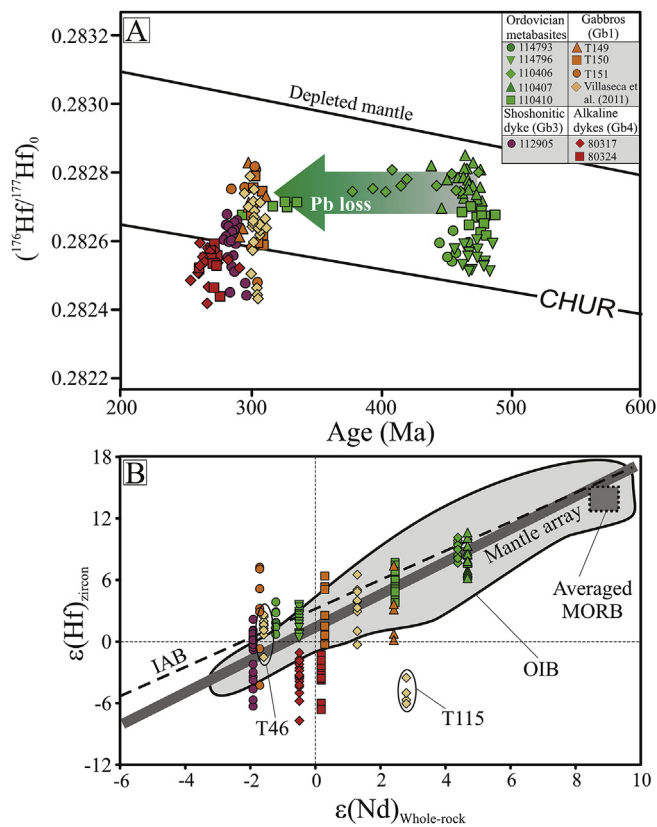

Fig. 8. (A) Initial $^{176}Hf/^{177}Hf$ vs. single U–Pb age for zircons from the analysed SCS mafic rocks. (B) εHf in zircon analyses vs. whole-rock εNd. Previous data on other Variscan gabbros (Villaseca et al., 2011) has been included for comparison. Mantle array, OIB field and average MORB composition after Chauvel et al. (2008). The evolution line of IAB is from Vervoort and Blichert–Toft (1999).

some, making their association with an specific geodynamic setting unclear (Variscan cycle, pre-Atlantic rifting).

Our geochronological results, based on both U–Pb zircon and
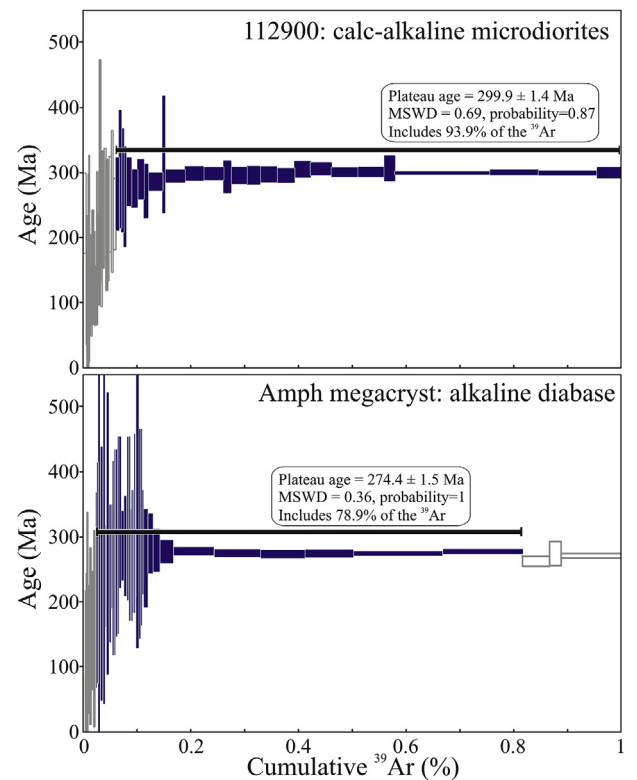
Fig. 9. $^{40}Ar/^{39}Ar$ plateau diagrams for incremental heating experiments on single amphibole crystals from microdiorite 112900 and a kaersutite megacryst from an alkaline diabase. Box heights are 2σ. Ages presented with 2σ uncertainty including a J-value = 0.00026948 ± 0.00000023 (sample 112900) and 0.00026926 ± 0.00000023 (kaersutite megacryst). Plateau steps are in dark blue; rejected steps are grey.

^{40}Ar–^{39}Ar ages, provide a more precise time frame for the entrainment of the post-collisional Permian magmas. The three gabbroic samples (T149, T150 and T151) show crystallisation ages (305–294 Ma; Fig. 7) within a range slightly wider than previously determined (307–300 Ma; Bea et al.,

2006; Zeck et al., 2007; Villaseca et al., 2011). Nevertheless, this data reinforces the coetaneous emplacement of mantle-derived magmas together with the voluminous SCS peraluminous felsic plutons (312–298 Ma; U–Pb in zircon; e.g., Gutiérrez–Alonso et al., 2011; Orejana et al., 2012; Díaz–Alvarado et al., 2013) during the late Variscan stages.

The age obtained for the microdiorite sample (299.9 ± 1.4 Ma) is close to that determined on an E–W granite porphyry dyke (296 ± 3 Ma; Galindo et al., 1994), overlapping the younger ages of granitic intrusions. This Gb2 mafic suite, and the accompanying more abundant E–W granitic porphyry dykes, crosscut the whole batholith (Villaseca et al., 2004), and their coeval intrusion is confirmed by mixing and mingling structures observed in field exposures (Huertas and Villaseca, 1994). Although they mostly postdate the main event of granite magma emplacement in the SCS, the above ages indicate that this bimodal suite of dykes can be considered contemporary with respect to the last SCS plutonism. In fact, there is evidence of these dyke swarms being interrupted by late granite plutons (e.g., Ubanell and Doblas, 1987). The age of 292.1 ± 1.8 Ma obtained from a N–S porphyry dyke sample (116452) which intersects the main E–W suite, implies that these felsic magmas followed the build-up of the SCS batholith for nearly 8 Myr (~300–292 Ma). They probably represent feeder conduits of shallow magma bodies or volcanic emissions. Volcanic and subvolcanic mafic and felsic igneous rocks of equivalent age (293–287 Ma) have been described to the east of the SCS (Lago et al., 2004 and references therein). The similitude in age between the gabbro T149 (294.4 ± 2.7 Ma; Fig. 7) and the bimodal suite of dykes suggests that the calc-alkaline Variscan gabbros and the microdiorite dyke swarms might represent mantle-derived magmas belonging to a single magmatic event which extended in the broad range of 307–294 Ma. Coeval mafic and felsic melts intruded in several pulses during this time span, with an initial stage characterised by pluton emplacement (up to ~298 Ma) and a subsequent phase of dyke intrusion. The age of the Gb3 monzonitic gabbro dykes (285.6 ± 1.4 Ma; Fig. 6) is younger than that of the previous microdiorites. Moreover, these potassic (shoshonitic) gabbros are also accompanied by low volume felsic magmas and represent a localised minor magmatic event within the SCS. Taking all this into account, these mafic dykes might be seen as the final magmatic manifestation of the Variscan cycle in the SCS.

A gap of about 10 Myr precedes the onset of alkaline magmatism. This group of dykes was thought to intrude mainly around 264 Ma (Ar–Ar in amphibole; Perini et al., 2004; Scarrow et al., 2006; Perini and Timmerman, 2008), however, these studies were focused exclusively on the ultramafic lamprophyre types, leaving aside a suite of mafic diabases, which exhibit a distinct isotopic composition (Fig. 4; Orejana et al., 2008). These diabases did not provide magmatic zircons, so we performed Ar–Ar on the abundant kaersutite megacrysts they carry, which are clearly cogenetic, as demonstrated by the isotopic data (Orejana et al., 2006). The Ar–Ar age of 274.4 ± 1.5 Ma (Fig. 9) obtained from this amphibole suggests that the Gb4 alkaline event started 10 Myr sooner than previously thought and that the diabases are slightly older than the lamprophyres. The other two alkaline samples analysed (80317 and 80324) belong to a suite of intermediate to felsic monzonitic-syenitic dykes which are fractionated melts genetically related to the lamprophyric magmatism (Orejana and Villaseca, 2006). Their ages (265.4 ± 4.1 Ma and 271.0 ± 2.1 Ma) closely resemble that of the lamprophyres, reinforcing the mentioned relationship. This data is significantly older than a previous age obtained from another alkaline Gb4 syenitic dyke (252 ± 3.0 Ma; Fernández–Suárez et al., 2006), although this is an intercept age derived from a small number of analyses (*n* = 5). In any case, our geochronological data would favour the presence of several stages of alkaline magma input within the narrow range of 274–264 Ma, rather than a single pulse.

The occurrence of this Permian alkaline magmatism is probably associated with a transitional geodynamic scenario involving lithosphere thinning and the upwelling of a deeper mantle (Orejana et al., 2008), during a rifting stage previous to the development of the Central Atlantic Magmatic Province. The onset of tholeiitic magmatism (Messejana–Plasencia dyke) around the Triassic–Jurassic limit (203 ± 3 Ma; Dunn et al., 1998) took place after a prolonged lapse of magmatic quiescence in the SCS. This large dyke has been linked to the opening of the Atlantic Ocean after impingement of the Central Atlantic mantle plume, channelled towards the NE (e.g., Cebriá et al., 2003 and references therein).

8.2. Depth of melt extraction

The value of the $(Gd/Yb)_N$ ratio of mafic rocks provides a qualitative approximation to the depth of extraction of the Variscan and post-Variscan mafic primary magmas, showing that only the alkaline suite (Gb4) attained equilibrium with garnet (Fig. 3B), which implies minimum pressures in the order of 2.6–3 GPa (~80–100 km) (estimated at 1400–1500 °C on the basis of spinel-garnet equilibrium in peridotite xenoliths; e.g., Klemme and O'Neill, 2000; Green, 2015). The Variscan microdiorites and gabbros (Gb1 and Gb2 suites) display lower $(Gd/Yb)_N$ ratios and were probably formed by partial melting of a spinel lherzolite protolith, whereas the shoshonitic dykes have intermediate $(Gd/Yb)_N$ ratios, indicative of spinel ± garnet lherzolite conditions (Fig. 3B). The Ordovician metabasites will not be considered here, as the metamorphic imprint might have affected their chemistry, leading to ambiguous results.

We also considered the geothermobarometry approach of Lee et al. (2009), which estimates the *P–T* conditions of basaltic melt extraction in equilibrium with a peridotite. The input data for this calculation was the primary magma composition estimated for a set of selected samples using the algorithm of Herzberg and Asimow (2015). The resulting pressures, although providing wide ranges, are generally higher for the alkaline suite (mainly 3.9–5.6 GPa) when compared to the rest of mafic intrusions (mostly < 3.6 GPa) (Fig. 10). The post-Variscan alkaline lamprophyres and diabases might thus be of asthenospheric origin, whereas the Variscan suites are probably derived from a lithospheric mantle. The shoshonitic dykes have higher melting P values than the Gb2 microdiorites, in accordance with their higher $(Gd/Yb)_N$ ratios, indicating that their primary magmas must have been in equilibrium with a spinel-garnet lherzolite protolith.

The temperatures estimated for the bulk of the SCS mafic suites using Lee et al. (2009) thermometry (1350–1710 °C) are in accordance with a high geothermal gradient (>120 mW/m^2), however, this geothermobarometer is not calibrated for CO_2-bearing magmas and certain over-estimation of temperature and pressure is likely, respectively, for fertile mantle sources and magma H_2O contents higher than 2 wt.% (Lee et al., 2009). The presence of volatiles in the SCS mafic magmas can be deduced from the relative abundance of hydrous minerals in the studied rocks (Orejana et al., 2008, 2009). This is most evident in the alkaline suite, which shows "loss on ignition" values in the range 3–7 wt.% and presents high modal amounts of magmatic hydrous and carbonated minerals (Orejana et al., 2008). We thus consider our results as maximum estimated *P–T* conditions for initial mantle melting. The use of a thermometer based only on the liquid composition (Putirka, 2008; P-independent) yields a moderate reduction in T values (10–150 °C lower) with respect to Lee's estimations (1350–1535 °C) (Fig. 10), however, even lower temperatures might be expected if phlogopite was involved in the partial melting within the asthenospheric mantle (it is unstable over 1350 °C, Condamine et al., 2016).

Despite the uncertainty in the *P–T* estimates, upper mantle temperatures during late-Variscan stages (considering data from Gb1, Gb2 and Gb3 suites) were probably higher than the current geothermal estimations for the Spanish Central System (84 mW/m^2, Jiménez–Díaz et al., 2012) (Fig. 10). High heat flow at the end of the Variscan cycle is expected, considering the high-T conditions calculated for the SCS lower crustal granulites (~900–1000 °C, Zr-in-rutile and Ti-in zircon; Orejana et al., 2011), while the younger alkaline lamprophyres and diabases define a slightly cooler geotherm after the Variscan cycle (Fig. 10).

In any case, the estimated temperatures do not favour the melting of a
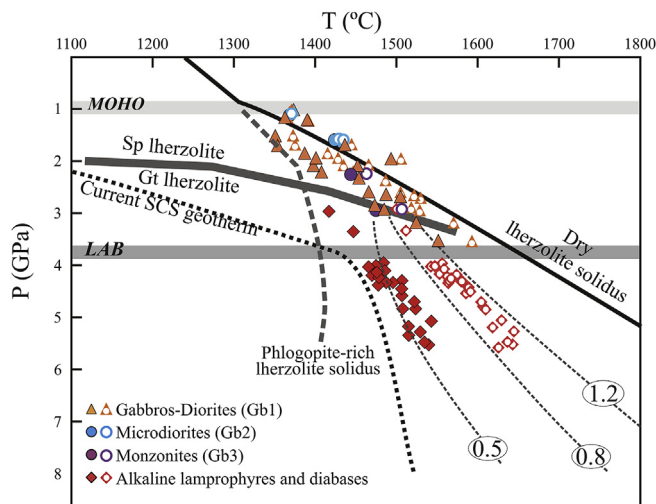
Fig. 10. Pressure and temperature estimations for the SCS mafic rocks. Two sets of data have been represented, both showing the same pressure estimation (based on Lee et al., 2009 geothermobarometer): full symbols illustrate temperatures estimated using the thermometer of Putirka (2008), whereas symbols with an inner white circle illustrate temperatures estimated using the thermobarometer of Lee et al. (2009). The dry lherzolite solidus and three solidus curves (thin grey dashed lines) for a CO_2-bearing lherzolite ($CO_2 = 0.15$ wt.%) have been taken from Gudfinnsson and Presnall (2005) and references therein. The numbers inside ovals for these latter solidus curves indicate the degree of melting. The phlogopite-rich lherzolite solidus curve was drawn after Condamine et al. (2016). The grey bar separating the spinel and garnet lherzolite stability fields was taken from Green (2015). The current SCS geotherm and the Moho and LAB (Lithosphere–Asthenosphere Boundary) depth were extracted from Jiménez–Díaz et al. (2012).

dry lherzolite, but rather a metasomatised mantle source. Pargasite amphibole, phlogopite or K-richterite, the first stable in the mantle below ~3 GPa and the other two at much higher pressures (Konzett and Ulmer, 1999; Fumagalli et al., 2009), might have played a role during melting. The water contained in these phases can produce a significant reduction in the solidus temperatures (e.g., Green, 2015; Condamine et al., 2016). A similar effect can be attributed to the presence of minor amounts of CO_2 in the mantle source, together with a low degree of melting (Gudfinnsson and Presnall, 2005). The involvement of CO_2 during melting is not clear in the case of the SCS shoshonitic and calc-alkaline suites, but small degrees of a CO_2-bearing lherzolite (e.g., $CO_2 = 0.15$ wt.%) melting would agree with the *P–T* estimations for the primary magmas of the alkaline dykes (Fig. 10), and explain their relatively high CO_2 contents (Orejana et al., 2008).

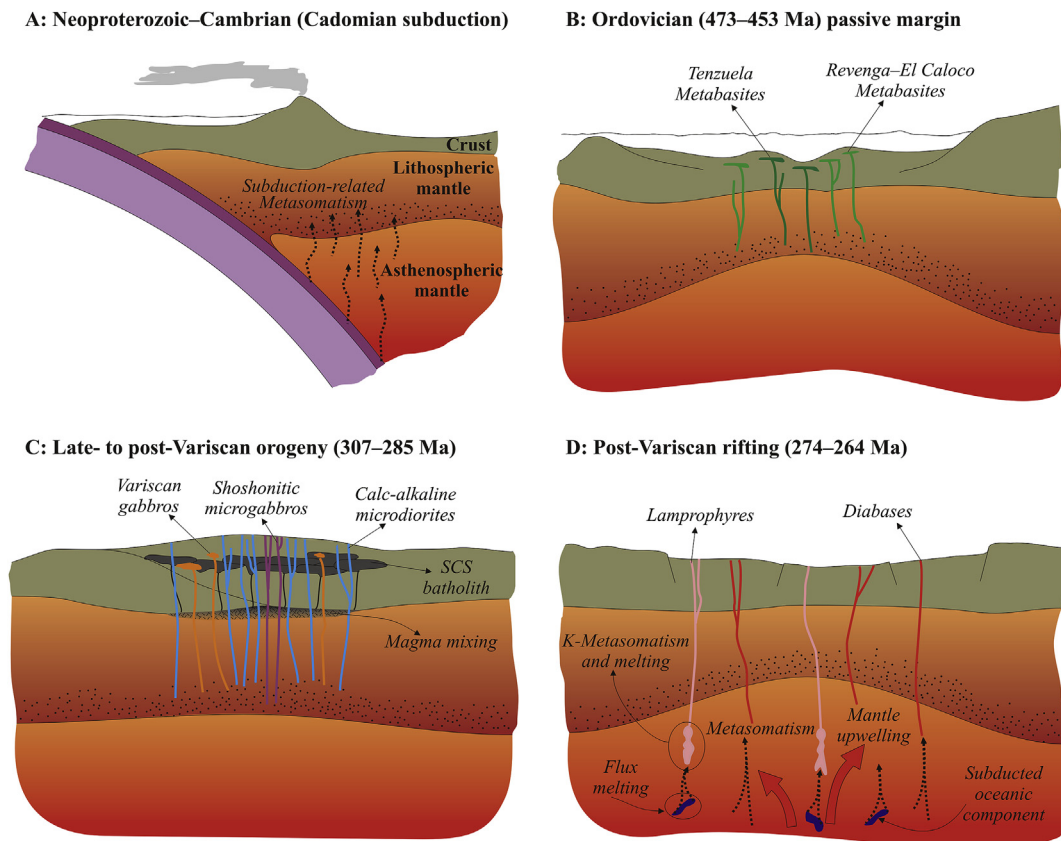### 8.3. Nature of the mantle sources: evolution over the Palaeozoic

According to the available dataset, the upper mantle under the SCS is characterised by a heterogeneous composition, ranging from an isotopically depleted (close to the MORB values) to a moderately enriched pole (Fig. 4A). Most of the suites of SCS mafic rocks have registered this heterogeneity internally, thus indicating that it has been present since the first manifestation of mantle-derived magmatism (Early Ordovician metabasites). These magmatic events show contrasting geochemical affinities (tholeiitic, calc-alkaline, shoshonitic, alkaline) (Fig. 2), however, which cannot be explained simply by differences in the melting conditions or en-route interaction with crustal components (assimilation, magma mixing). The composition of the mantle sources must have changed over time, and the effect of several enrichment processes has been proposed (Orejana et al., 2006, 2008, 2009, 2017; Orejana and Villaseca, 2008; Scarrow et al., 2009, 2011). It is important to note that only the most primitive mafic rocks within each suite are plotted in Figs. 3 and 4 and considered during the discussion, in order to reduce the

possible effects of fractionation and crustal contamination.

Some SCS Ordovician metabasites record the presence of a depleted mantle component with a geochemical signature similar to an E-MORB (Tenzuela sector; Orejana et al., 2017). The Hf isotope data of these samples also reflects a depleted nature (εHf > 4), whereas those determined on samples 114793 and 114796 (Revenga–El Caloco sector) are clearly lower (εHf < 4; Fig. 8B) and point to a derivation from a more enriched mantle source. This enrichment is also apparent in the trace element geochemistry of these rocks, which displays relatively high LILE (Fig. 2D). The negative Nb–Ta anomalies, Pb peaks and high Th/Yb ratios (Figs. 2D and 3A) indicate the involvement of a crustal imprint, as previously suggested (Villaseca et al., 2015; Orejana et al., 2017). The melting of a subduction-related mantle source might explain the more radiogenic Hf isotope ratios of samples 114793 and 114796, which overlap the evolution line of Island-Arc Basalts (IAB) (Fig. 8B). The higher εHf values of these samples relative to the mantle array also agree with this possibility, as pelagic sediments have high Lu/Hf ratios, along with low Sm/Nd ratios (e.g., Patchett et al., 1984). The proximity of the Iberian Massif to the Cadomian continental arc, active from ~750 Ma to 540 Ma (Linnemann et al., 2007) in the northern margin of Gondwana, makes a subduction imprint within the upper mantle possible (Fig. 11A). A process of crustal thickening associated with a subduction-collision stage has also been suggested for the generation of a large S-type Cambrian–Early Ordovician granite batholith in the SCS, but taking place previously to the passive margin sedimentation during Floian (500–478 Ma; Villaseca et al., 2016). Subsequent lithosphere thinning and mantle upwelling during Early to Late Ordovician, in the framework of this passive margin setting (oceanic rifting), probably involved the low pressure melting of two distinct lithospheric mantle sources: a depleted (Tenzuela metabasites) and a slightly enriched (Revenga–El Caloco metabasites) component (Fig. 11B).

The suite of gabbroic intrusions associated with the Variscan orogeny shows a markedly heterogeneous Hf isotope record (Fig. 8B). The deviation of this data from the mantle array probably results from assigning a single value of radiogenic Nd (the average whole-rock composition) to the variable Hf ratios extracted from a set of zircon crystals. Such heterogeneity in magmatic zircons within a single sample (up to 11 epsilon units) can only be explained by an open-system process. Similar wide εHf values have been interpreted as evidence of the mixing of magmas from crustal and mantle sources (e.g., Sun et al., 2010; Tang et al., 2014). Mixing with felsic magmas has been recognised in several SCS mafic intrusions, and is manifested in the formation of lithologies of intermediate composition (Q-diorites, tonalites) (Orejana et al., 2009; Molina et al., 2012). Based on these observations, Villaseca et al., 2011 related the εHf variation in zircon from gabbros with a process of magma mixing, which might be consistent with data from sample T115, which plots well below the mantle evolution line (Fig. 8B). The three analysed gabbros (T149, T150 and T151), however, are basic in composition (SiO_2 < 49 wt.%; Orejana et al., 2009) and do not show petrographic evidence of interaction with felsic magmas. Alternatively, zircons with contrasting isotope signatures might have been mixed during the storage of distinct mantle-derived magma batches in deep magma chambers or at the emplacement level. The moderately depleted to slightly enriched Nd isotopic composition of the SCS gabbros is broadly similar to the Hf isotopes of the zircons they include (Fig. 8B). The continuous variation shown by the Sr–Nd–Hf isotopic systems might be inherited from a heterogeneous source region, due to the melting of a variably enriched mantle and the subsequent hybridisation of the accreted melts (although mixing with felsic magmas might have played a role in some cases).

The Sr–Nd isotope composition of the Gb1 gabbros is similar to other Variscan mafic rocks in nearby regions (northern Portugal, Galicia, Pyrenees) and overlaps the composition of peridotite xenoliths included in alkaline mafic volcanics from western and central Europe (Fig. 4A). The nature of the Iberian mantle enrichment admits at least two non-exclusive origins: (1) the imprint from ancient subduction (as hypothesised for the SCS metabasites), and (2) post-collisional crustal recycling.

A: Neoproterozoic–Cambrian (Cadomian subduction)

B: Ordovician (473–453 Ma) passive margin

C: Late- to post-Variscan orogeny (307–285 Ma)

D: Post-Variscan rifting (274–264 Ma)

Fig. 11. Schematic cartoon of the geodynamic evolution of the lithosphere under the Spanish Central System, representing the Cadomian orogeny (A), the Ordovician passive margin setting (B), the late- to post-Variscan context (C) and the continental rifting previous to the opening of the Atlantic ocean (D). Symbols and terms in Picture A apply to the rest of the drawings.

This latter possibility would require the delamination of a dense lower crustal root, and it has been suggested that this process shortly preceded the generation of the late Variscan mafic magmatism (e.g., Orejana et al., 2009). The present geochemical data does not allow a straightforward conclusion regarding this issue, but the fact that the gabbros with the least radiogenic Nd values (e.g., samples T46 and T151) plot predominantly above the mantle array, does not clearly support the recycling of a continental crustal component (εHf < 0), even if it happened immediately after the Variscan crustal thickening. Instead, the signatures of enriched mantle sources could reflect an older subduction of pelagic sediments (Fig. 11C), as discussed above for the Revenga–El Caloco metabasites.

The Gb2 suite of microdioritic dykes did not provide Hf isotope data from magmatic zircons. Nevertheless, their whole-rock composition closely resembles that of the Gb1 gabbros in terms of major and trace element contents (Figs. 2 and 3), and our geochronological data indicates that they can be considered coeval with the late mafic Variscan magmatism. Accordingly, they are probably the melting products of an enriched lithospheric mantle similar to that suggested for the Variscan gabbros. The isotopic composition of these microdiorites demonstrates high values of radiogenic Sr, resembling those of the dioritic terms of the Gb1 intrusions (Fig. 4), suggesting local mixing with felsic magmas (associated granite porphyry dykes).

The following melting episode in the SCS at ~284 Ma (Gb3 dykes) was a localised event, which mobilised a low volume of magma (Fig. 1). The geochemical features of these monzogabbros (shoshonitic affinity, high LILE and LREE concentrations, negative Nb anomalies and moderately enriched radiogenic ratios) (Figs. 2–4) would agree with the melting of a lithospheric mantle with a crustal imprint. The isotopic similarities with respect to the Gb1 and Gb2 suites imply that, in essence, a similar mantle source was involved to generate the monzogabbros. The

higher pressure estimations, K_2O content and $(Gd/Yb)_N$ ratios of these mafic rocks, however, when compared to the previous Variscan calc-alkaline intrusions (Figs. 2C and 3B), point to a slightly deeper level of melting within the spinel-garnet stability field. Shoshonitic magmas typically form during the last extensional stages of collisional orogens (e.g., Dewey, 1988) and have been ascribed to the melting of a subcontinental lithospheric mantle enriched by subduction-related fluids or melts (e.g., Foley, 1992; Turner et al., 1996; Yang et al., 2007). The K-rich character of the Gb3 suite implies a K-bearing phase in the source. The increasing Ce/Nb ratios for almost constant Nb/Th values, which is a tendency shared with the calc-alkaline suites (Fig. 12), suggests that amphibole was the main hydrous phase in the source, as can be deduced from the trace element composition of metasomatic minerals from mantle xenoliths (e.g., Ionov et al., 1997). The strong LREE enrichment shown by the Gb3 microgabbros (Fig. 2D) suggests that amphibole played a key role during the melting reaction. The association of shoshonites with the metasomatic agents of oceanic or continental derivation is a matter of debate and seems to be affected by the geodynamic context (e.g., Zhao et al., 2009; Lustrino et al., 2011). The range of radiogenic Hf in zircons from the Gb3 suite is centred on the mantle array (Fig. 8B), but constitutes a relatively scattered dataset which is in agreement with the melting of a mantle source with a variable degree of enrichment (εHf from +2.1 to −6.3). The similitude in the radiogenic Hf values of sample 112905 with respect to data from the Gb1 intrusions favours a metasomatic imprint associated with the infiltration of subduction-related fluids-melts (Fig. 11C), as discussed above for the Variscan gabbros and the Ordovician metabasites. Accordingly, the observed enrichment of the lithospheric mantle under central Spain was mainly attained during the Cadomian orogeny, and persisted to the end of the Variscan collision.

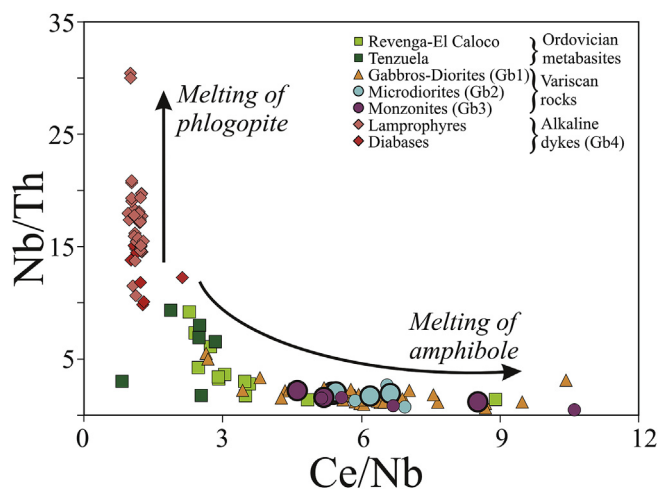The SCS Gb4 alkaline dyke suite is the last Palaeozoic mafic magmatic

Fig. 12. Nb/Th vs. Ce/Nb ratios of SCS mantle-derived rocks. Smaller symbols are data from the literature (see references in caption to Fig. 2). The arrows indicate the predicted change in melt composition due to partial melting of an amphibole- or phlogopite-bearing peridotite.

event in the region. This magmatic event is also significant for its OIB-like geochemistry, illustrative of its derivation from asthenospheric mantle sources, and because it marks the transition from orogenic to anorogenic magmatism in central Iberia (Orejana et al., 2008). Our geochronological data and previous geochemical studies (Orejana et al., 2006, 2008) reveal that it can be divided in two groups: (1) isotopically depleted sodic diabases, and (2) slightly enriched potassic lamprophyres (camptonites)–monzosyenites, which intruded from 274 Ma (diabases) to mainly 264 Ma (lamprophyres). Both groups show broadly similar trace element contents, characterised by high LILE, HFSE and LREE concentrations and strong positive Nb anomalies (Figs. 2 and 3B). These features are in accordance with mantle sources metasomatised by volatile-alkali-rich melts, and the high REE contents and Rb/Sr ratios shown by the isotopically depleted dykes imply that melting occurred shortly after metasomatism (Orejana et al., 2008). A main feature of the two analysed alkaline dykes is the low εHf values (−1.1 to −7.7; Supplementary Table 4) associated with whole-rock εNd numbers from +0.2 to −0.5 (Fig. 8B). The fact that the radiogenic Nd data represents average values, implies that even more positive εNd figures might be related to some of the Hf zircon data, which would move these points further apart from the mantle evolution line. We interpret this as an indication of decoupling in the Hf–Nd isotopic space. Such decoupling has been identified in different alkaline ultramafic rocks (e.g., kimberlites, ultramafic lamprophyres and lamproites), and related to the melting of mantle sources metasomatised either by crustal-derived zircon-bearing sediments (Prelević et al., 2010) or by alkaline melts extracted from subducted oceanic crust (e.g., Nowell et al., 2004; Tappe et al., 2011, 2013). The first possibility has been proposed for lamproites showing a clear crustal imprint: high radiogenic Sr, low εHf–εNd, and incompatible trace element ratios similar to upper crust values (e.g., Ce/Pb, Nb/U). The SCS alkaline dykes do not show such enriched signatures in their isotopic (Fig. 4) or elemental (Fig. 3A) composition, indicating the involvement of deep metasomatic agents (Orejana et al., 2008). The slight Hf–Nd decoupling could be ascribed to the melting of (or interaction with) a mantle component which evolved with time-integrated low Lu/Hf relative to Sm/Nd (Griffin et al., 2000; Nowell et al., 2004). The recycling of oceanic lithosphere deep in the mantle has been proposed as a possible source for the addition of such a signature (e.g., Tappe et al., 2013). Upwelling of the asthenospheric mantle in the context of continental rifting might have allowed this kind of subducted material to ascend and be CO_2- and H_2O-flux melted (Fig. 11D). This melt influx would have caused modal metasomatism in the form of veins containing volatile-rich minerals (e.g., phlogopite, apatite, carbonate). Metasomatic veins generally have lower

melting temperatures compared with the surrounding peridotite (e.g., Foley et al., 1999), so they would have been preferentially consumed during the melting event, thus imprinting the Nd–Hf isotopic mismatch to the magma. The geochemistry of these alkaline lamprophyres and associated monzosyenites is in agreement with derivation from a phlogopite-bearing mantle (Fig. 12), whereas the diabases represent the input of magmas from a convecting mantle with a different paragenesis of metasomatic phases (Orejana et al., 2008).

Although Nd model ages are not significant from a quantitate standpoint, as the metasomatised nature of the mantle sources imply that they only represent minimum ages from a mixture of components, a qualitative approach can provide interesting data. It is relevant that Nd model ages of the SCS mafic magmas, up to the end of the Variscan cycle, overlap in the range of 1130–2100 Ma (Fig. 4B), suggesting that they were extracted from a broadly similar lithospheric mantle region. By contrast, the Gb4 alkaline suite shows lower Nd model ages, supporting the ascent of a deeper (and younger) convecting asthenospheric mantle in the context of continental rifting. The different Nd model ages of diabases (452–614 Ma) and lamprophyres (840–1126 Ma) (Fig. 4B) demonstrate that an old recycled component played a key role in the genesis of this latter group of dykes.

9. Conclusions

Zircon U–Pb isotopes and Ar–Ar geochronology on amphibole have allowed the accurate dating of several Variscan and post-Variscan suites of mafic magmatic rocks from the Spanish Central System. The Variscan gabbros have provided ages (305–294 Ma) similar to those of the large Variscan granitic batholith (312–298 Ma), but slightly younger than previous geochronological data on SCS gabbro massifs. The youngest data overlaps the ages of a suite of mafic (microdiorites; 299 Ma) and felsic (granitic porphyries; 292 Ma) dykes. The geochronological and geochemical similarities shown by these two groups of mafic rocks indicate that the late Variscan igneous activity in the SCS was characterised by a bimodal magmatism involving prevalent crustal peraluminous melts and subordinated mafic-intermediate calc-alkaline series. The later subvolcanic shoshonitic magmas (285 Ma) mark the end of the Variscan orogenic cycle. Alkaline diabases and lamprophyres have shown differences in their age of intrusion (274 Ma and 271–265 Ma, respectively) in a way that matches their isotopic signatures.

Pressure and temperature estimations indicate that the Permian alkaline magmas were extracted from asthenospheric mantle sources, whereas the previous Variscan suites of mafic rocks were derived from the melting of a shallower lithospheric mantle. Temperatures, although poorly constrained, support a higher geothermal gradient at the end of the Variscan cycle when compared with the later Permian rifting setting. The lithospheric mantle under the SCS seems to have been affected mainly by the recycling of clay-rich sediments via oceanic subduction (associated with the Cadomian orogeny), inducing more radiogenic Hf values. This mantle was probably the source of the mafic igneous suites exhibiting an enriched isotopic composition and trace element ratios typical of crustal components: pre-Variscan (Ordovician) Revenga–El Caloco metabasites and Variscan calc-alkaline and shoshonitic series. The entrainment of a deeper (asthenospheric) mantle is restricted to extensional geodynamic settings with significant mantle upwelling, marking the onset of successive anorogenic magmatic events in Iberia. This is the case for the Permian alkaline dykes, which show heterogeneous radiogenic Nd values (εNd from +7 to −1) and OIB-like trace element signatures. The moderate decoupling of the Hf–Nd radiogenic values observed in the enriched alkaline dykes could be related to a mantle component which evolved with time-integrated low Lu/Hf relative to Sm/Nd. A possible candidate would be a deep-seated metasomatic melt generated from a recycled oceanic lithosphere. This agent might have ascended due to mantle upwelling, finally giving rise to a phlogopite-bearing vein network. The subsequent melting of this metasomatised mantle would have transferred the decoupled isotopic ratios to the mafic magmas.

Declaration of competing interest

Acknowledgements

Appendix A. Supplementary data

Supplementary data to this article can be found online at https://doi.org/10.1016/j.gsf.2020.01.002.

References

Amelin, Y., Lee, D.C., Halliday, A.N., 2000. Early-middle Archaean crustal evolution deduced from Lu-Hf and U–Pb isotopic studies of single zircon grains. Geochem. Cosmochim. Acta 64, 4205–4225.

Barbero, L., Villaseca, C., 2000. Eclogite facies relics in metabasites from the Sierra de Guadarrama (Spanish Central System); P-T estimations and implications for the Hercynian evolution. Mineral. Mag. 64, 815–836.

Bea, F., Montero, P., González-Lodeiro, F., Talavera, C., Molina, J.F., Scarrow, J.H., Whitehouse, M.J., Zinger, T., 2006. Zircon thermometry and U–Pb ion-microprobe dating of the gabbros and associated migmatites of the Variscan Toledo anatectic complex, central Iberia. J. Geol. Soc. Lond. 163, 847–855.

Bea, F., Montero, P., Molina, J.F., 1999. Mafic precursors, peraluminous granitoids, and late lamprophyres in the Avila batholith; a model for the generation of Variscan batholiths in Iberia. J. Geol. 107, 399–419.

Beccaluva, L., Bianchini, G., Bonadiman, C., Siena, F., Vaccaro, C., 2004. Coexisting anorogenic and subduction-related metasomatism in mantle xenoliths from the Betic Cordillera (southern Spain). Lithos 75, 67–87.

Black, L.P., Gulson, B.L., 1978. The age of the Mud Tank carbonatite, strangways range, northern territory. BMR J. Aust. Geol. Geophys. 3, 227–232.

Black, L.P., Kamo, S.L., Allen, C.M., Aleinikoff, J.N., Davis, D.W., Korsch, R.J., Foudoulis, C., 2003. TEMORA 1: a new zircon standard for Phanerozoic U–Pb geochronology. Chem. Geol. 200, 155–170.

Black, L.P., Kamo, S.L., Allen, C.M., Davis, D.W., Aleinikoff, J.N., Valley, J.W., Mundil, R., Campbell, I.H., Korsch, R.J., Williams, I.S., Foudoulis, C., 2004. Improved $^{206}Pb/^{238}U$ microprobe geochronology by the monitoring of a trace-element-related matrix effect; SHRIMP, ID–TIMS, ELA–ICP–MS and oxygen isotope documentation for a series of zircon standards. Chem. Geol. 205, 115–140.

Bouvier, A., Vervoort, J.D., Patchett, P.J., 2008. The Lu–Hf and Sm–Nd isotopic composition of CHUR: constraints from unequilibrated chondrites and implications for the bulk composition of terrestrial planets. Earth Planet. Sci. Lett. 273, 48–57.

Cebriá, J.M., López–Ruiz, J., Doblas, M., Martins, L.T., Munha, J., 2003. Geochemistry of the early Jurassic Messejana–Plasencia dyke (Portugal–Spain); implications on the origin of the central Atlantic magmatic province. J. Petrol. 44, 547–568.

Chauvel, C., Lewin, E., Carpentier, M., Arndt, N., Marini, J.C., 2008. Relationships between Lu–Hf and Sm–Nd isotopic systems in the global sedimentary system. Nat. Geosci. 1, 64–67.

Chen, B., Tian, W., Jahn, B.M., Chen, Z.C., 2008. Zircon SHRIMP U–Pb ages and in-situ Hf isotopic analysis for the Mesozoic intrusions in South Taihang, North China craton: evidence for hybridization between mantle-derived magmas and crustal components. Lithos 102, 118–137.

Cheong, C.-S., Kim, N., Jo, H.J., Cho, M., Choi, S.H., Zhou, H., Geng, J.-Z., 2015. Lithospheric mantle signatures as revealed by zircon Hf isotopes of Late Triassic post-collisional plutons from the central Korean peninsula, and their tectonic implications. Terra. Nova 27, 97–105.

Condamine, P., Médard, E., Devidal, J.-L., 2016. Experimental melting of phlogopite-peridotite in the garnet stability field. Contrib. Mineral. Petrol. 171, 95.

Couzinié, S., Laurent, O., Moyen, J.F., Zeh, A., Bouilhol, P., Villaros, A., 2016. Post-collisional magmatism: crustal growth not identified by zircon Hf–O isotopes. Earth Planet. Sci. Lett. 456, 182–195.

Dai, L.-Q., Zhao, Z.-F., Zheng, Y.-F., Li, Q., Yang, Y., Dai, M., 2011. Zircon Hf–O isotope evidence for crust–mantle interaction during continental deep subduction. Earth Planet. Sci. Lett. 308, 229–244.

Dewey, J.F., 1988. Extensional collapse of orogens. Tectonics 7, 1123–1139.

Dias, G., Leterrier, J., 1994. The genesis of felsic-mafic plutonic associations: a Sr and Nd isotopic study of the Hercynian Braga Granitoid Massif (Northern Portugal). Lithos 32, 207–223.

Dias, G., Simões, P.P., Ferreira, N., Leterrier, J., 2002. Mantle and crustal sources in the genesis of late-Hercynian granitoids (NW Portugal): geochemical and Sr–Nd isotopic constraints. Gondwana Res. 5, 287–305.

Díaz Alvarado, J., Fernández, C., Castro, A., Moreno–Ventas, I., 2013. SHRIMP U–Pb zircon geochronology and thermal modeling of multilayer granitoid intrusions. Implications for the building and thermal evolution of the Central System batholith, Iberian Massif, Spain. Lithos 175–176, 104–123.

Duncan, R.A., Keller, R.A., 2004. Radiometric ages for basement rocks from the emperor seamounts, ODP Leg 197. Geochem. Geophys. Geosyst. 5, Q08L03.

Dunn, A.M., Reynolds, P.H., Clarke, D.B., Ugidos, J.M., 1998. A comparison of the age and composition of the Sherburne dyke, Nova Scotia, and the Messejana dyke, Spain. Can. J. Earth Sci. 35, 1110–1115.

Elburg, M.A., Andersen, T., Bons, P.D., Simonsen, S.L., Weisheit, A., 2013. New constraints on Phanerozoic magmatic and hydrothermal events in the Mt Painter Province, south Australia. Gondwana Res. 24, 700–712.

Fernández Suárez, J., Arenas, R., Jeffries, T.E., Whitehouse, M.J., Villaseca, C., 2006. A U–Pb study of zircons from a lower crustal granulite xenolith of the Spanish Central system: a record of Iberian lithospheric evolution from the Neoproterozoic to the Triassic. J. Geol. 114, 471–483.

Foley, S.F., 1992. Petrological characterization of the source components of potassic magmas: geochemical and experimental constraints. Lithos 28, 187–204.

Foley, S.F., Musselwhite, D.S., Van der Laan, S.R., 1999. Melt compositions from ultramafic vein assemblages in the lithospheric mantle a comparison of cratons and non-cratonic settings. In: Gurney, J.J., Gurney, J.L., Pascoe, M.D., Richardson, S.H. (Eds.), Proceedings of the 7th International Kimberlite Conference, South Africa, 1998. National Book Printers, Cape Town, pp. 228–246.

Fumagalli, P., Zanchetta, S., Poli, S., 2009. Alkali in phlogopite and amphibole and their effects on phase relations in metasomatized peridotite: a high pressure study. Contrib. Mineral. Petrol. 158, 723–737.

Galán, G., Pin, C., Duthou, J.L., 1996. Sr–Nd isotopic record of multi-stage interactions between mantle-derived magmas and crustal components in a collision context the ultramafic-granitoid association from Vivero (Hercynian belt, NW Spain). Chem. Geol. 131, 67–91.

Galindo, C., Huertas, M.J., Casquet, C., 1994. Cronología Rb–Sr y K–Ar de diques de la Sierra de Guadarrama (Sistema Central Español). Geogaceta 16, 23–26 (in Spanish).

Gardiner, N.J., Kirkland, C.L., van Kranendonk, M.J., 2016. The juvenile hafnium isotope signal as a record of supercontinent cycles. Sci. Rep. 6, 38503.

Green, D.H., 2015. Experimental petrology of peridotites, including effects of water and carbon on melting in the Earth's upper mantle. Phys. Chem. Miner. 42, 95–122.

Griffin, W.L., Belousova, E.A., Shee, S.R., Pearson, N.J., O'Reilly, S.Y., 2004. Archean crustal evolution in the northern Yilgarn Craton: U–Pb and Hf–isotope evidencefrom detrital zircons. Precambrian Res. 131, 231–282.

Griffin, W.L., Pearson, N.J., Belousova, E.A., Jackson, S.E., O'Reilly, S.Y., van Achterberg, E., Shee, S.R., 2000. The Hf isotope composition of cratonic mantle: LAM-MC-ICPMS analysis of zircon megacrysts in kimberlites. Geochem. Cosmochim. Acta 64, 133–147.

Griffin, W.L., Pearson, N.J., Belousova, E.A., Saeed, A., 2006. Comment: Hf-isotope heterogeneity in zircon 91500. Chem. Geol. 233, 358–363.

Griffin, W.L., Pearson, N.J., Belousova, E.A., Saeed, A., 2007. Reply to "Comment to short communication 'Comment: Hf-isotope heterogeneity in zircon 91500' by Griffin, W.L., Pearson, N.J., Belousova, E.A., Saeed, A., (Chemical Geology 233 (2006) 358–363)" by F. Corfu. Chem. Geol. 244, 354–356.

Gudfinnsson, G.H., Presnall, D.C., 2005. Continuous gradations among primary carbonatitic, kimberlitic, melilititic, basaltic, picritic, and komatiitic melts in equilibrium with garnet lherzolite at 3–8 GPa. J. Petrol. 46, 1645–1659.

Gutiérrez Alonso, G., Fernández Suárez, J., Jeffries, T.E., Johnston, S.T., Pastor–Galán, D., Murphy, J.B., Franco, M.P., Gonzalo, J.C., 2011. Diachronous post-orogenic magmatism within a developing orocline in Iberia, European Variscides. Tectonics 30, TC5008.

Heinonen, A.P., Andersen, T., Rämö, O.T., 2010. Re-evaluation of rapakivi petrogenesis: source constraints from the Hf isotope composition of zircon in the rapakivi granites and associated mafic rocks of southern Finland. J. Petrol. 51, 1687–1709.

Herzberg, C., Asimow, P.D., 2015. PRIMELT3 MEGA.XLSM software for primary magma calculation: peridotite primary magma MgO contents from the liquidus to the solidus. Geochem. Geophys. Geosyst. 16, 563–578.

Huertas, M.J., 1990. Las asociaciones filonianas tardihercínicas en la Sierra de Guadarrama (Sistema Central Español). Ph.D. thesis, UCM, Madrid, p. 335 (in Spanish).

Huertas, M.J., Villaseca, C., 1994. Les derniers cycles magmatiques posthercyniens du système central espagnol: les essaims filoniens calco-alcalins. Schweizerische Mineralogische und Petrographische Mitteilungen 74, 383–401 (in French).

Ionov, D.A., Griffin, W.L., O'Reilly, S.Y., 1997. Volatile-bearing minerals and lithophile trace elements in the upper mantle. Chem. Geol. 141, 153–184.

Jiménez–Díaz, A., Ruiz, J., Villaseca, C., Tejero, R., Capote, R., 2012. The thermal state and strength of the lithosphere in the Spanish Central System and Tajo Basin from crustal heat production and thermal isostasy. J. Geodyn. 58, 29–37.

Klemme, S., O'Neill, H.S.C., 2000. The near-solidus transition from garnet lherzolite to spinel lherzolite. Contrib. Mineral. Petrol. 138, 237–248.

Konzett, J., Ulmer, P., 1999. The stability of hydrous potassic phases in lherzolitic mantle-an experimental study to 9.5 GPa in simplified and natural bulk compositions. J. Petrol. 40, 629–652.

Koppers, A.A.P., 2002. ArArCALC – software for $^{40}Ar/^{39}Ar$ age calculations. Comput. Geosci. 28, 605–619.

Kuiper, K.F., Deino, A., Hilgen, F.J., Krijgsman, W., Renne, P.R., Wijbrans, J.R., 2008. Synchronizing rock clocks of Earth history. Science 320, 500–504.

Lago, M., Arranz, E., Gil, A., Pocovi, A., 2004. Cordilleras ibérica y costero-catalana: magmatismo asociado. In: Vera, J.A. (Ed.), Geología de España. Sociedad Geológica de España – Instituto Geológico y Minero de España, Madrid, pp. 522–525 (in Spanish).

Lee, C.-T.A., Luffi, P., Plank, T., Dalton, H., Leeman, W.P., 2009. Constraints on the depths and temperatures of basaltic magma generation on Earth and other terrestrial planets using new thermobarometers for mafic magmas. Earth Planet. Sci. Lett. 279, 20–33.

Linnemann, U., Gerdes, A., Drost, K., Buschmann, B., 2007. The continuum between Cadomian Orogenesis and opening of the Rheic Ocean: constraints from LA-ICP-MS U–Pb zircon dating and analysis of plate-tectonic setting (Saxo-Thuringian Zone, NE Bohemian Massif, Germany). In: Linnemann, U., Nance, D., Kraft, P., Zulauf, G. (Eds.), The Evolution of the Rheic Ocean: from Avalonian–Cadomian Active Margin to Alleghenian–Variscan Collision. Geological Society of America, Special Paper., Boulder, Colorado, pp. 61–96.

Ludwig, K.R., 2003. ISOPLOT/Ex, Version 3. A Geochronological Toolkit for Microsoft Excel, vol. 4. Berkeley Geochronological Center Special Publication, pp. 1–71.

Ludwig, K.R., Mundil, R., 2002. Extracting reliable U–Pb ages and errors from complex populations of zircons from Phanerozoic tuffs. Geochem. Cosmochim. Acta 66 (Suppl. 1), 463.

Lustrino, M., Duggen, S., Rosenberg, C.L., 2011. The Central-Western Mediterranean: anomalous igneous activity in an anomalous collisional tectonic setting. Earth Sci. Rev. 104, 1–40.

McDonough, W.F., Sun, S.S., 1995. The composition of the Earth. Chem. Geol. 120, 223–253.

Min, K.W., Mundil, R., Renne, P.R., Ludwig, K.R., 2000. A test for systematic errors in ^{40}Ar/^{39}Ar geochronology through comparison with U/Pb analysis of a 1.1-Ga rhyolite. Geochem. Cosmochim. Acta 64, 73–98.

Molina, J.F., Montero, P.G., Bea, F., Scarrow, J.H., 2012. Anomalous xenocryst dispersion during tonalite–granodiorite crystal mush hybridization in the mid crust: mineralogical and geochemical evidence from Variscan appinites (Avila Batholith, Central Iberia). Lithos 153, 224–242.

Nowell, G.M., Pearson, D.G., Bell, D.R., Carlson, R.W., Smith, C.B., Kempton, P.D., Noble, S.R., 2004. Hf isotope systematics of kimberlites and their megacrysts: new constraints on their source regions. J. Petrol. 45, 1583–1612.

Orejana, D., Villaseca, C., 2006. Los diques alcalinos de pórfidos monzo-sieníticos del Sistema Central Español: relación con los diques lamprofídicos acompañantes. Geogaceta 40, 103–106 (in Spanish).

Orejana, D., Villaseca, C., 2008. Heterogeneous metasomatism in cumulate xenoliths from the Spanish Central System: implications on percolative fractional crystallization of lamprophyric melts. In: Coltorti, M., Grégoire, M. (Eds.), Metasomatism in Oceanic and Continental Lithospheric Mantle, vol. 293. Geological Society of London Special Publication, pp. 101–120.

Orejana, D., Villaseca, C., Paterson, B.A., 2006. Geochemistry of pyroxenitic and hornblenditic xenoliths in alkaline lamprophyres from the Spanish Central System. Lithos 86, 167–196.

Orejana, D., Villaseca, C., Billström, K., Paterson, B.A., 2008. Petrogenesis of Permian alkaline lamprophyres and diabases from the Spanish Central System and their geodynamic context within western Europe. Contrib. Mineral. Petrol. 156, 457–500.

Orejana, D., Villaseca, C., Pérez–Soba, C., López–García, J.A., Billström, K., 2009. The Variscan gabbros from the Spanish Central System: a case for crustal recycling in the sub-continental lithospheric mantle? Lithos 110, 262–276.

Orejana, D., Villaseca, C., Armstrong, R.A., Jeffries, T.E., 2011. Geochronology and trace element chemistry of zircon and garnet from granulite xenoliths: constraints on the tectonothermal evolution of the lower crust under central Spain. Lithos 124, 103–116.

Orejana, D., Villaseca, C., Valverde–Vaquero, P., Belousova, E.A., Armstrong, R.A., 2012. U–Pb geochronology and zircon composition of late Variscan S- and I-type granitoids from the Spanish Central System batholith. Int. J. Earth Sci. 101, 1789–1815.

Orejana, D., Villaseca, C., Merino Martínez, E., 2017. Basic ordovician magmatism of the Spanish central system: constraints on the source and geodynamic setting. Lithos 284–285, 608–624.

Patchett, P.J., Tatsumoto, M., 1980. Lu–Hf total-rock isochron for the eucrite meteorites. Nature 288, 571–574.

Patchett, P.J., White, W.M., Feldmann, H., Kielinczuk, S., Hofmann, A.W., 1984. Hafnium/rare earth fractionation in the sedimentary system and crust–mantle recycling. Earth Planet. Sci. Lett. 69, 365–378.

Perini, G., Timmerman, M.J., 2008. Permian ^{40}Ar/^{39}Ar ages for post-Variscan minor intrusions in the Iberian range and Spanish central system. Geol. Acta 6, 335–344.

Perini, G., Cebriá, J.M., López–Ruiz, J.M., Doblas, M., 2004. Carboniferous-Permian mafic magmatism in the variscan belt of Spain and France: implications for mantle sources. In: Wilson, M., Neumann, E.R., Davies, G.R., Timmerman, M.J., Heeremans, M., Larsen, B. (Eds.), Permo-Carboniferous Magmatism and Rifting in Europe, vol. 223. Geological Society of London Special Publication, pp. 415–438.

Prelević, D., Stracke, A., Foley F., S., Romer L., R., Conticelli, S., 2010. Hf isotope compositions of Mediterranean lamproites: Mixing of melts from asthenosphere and crustally contaminated mantle lithosphere. Lithos 119, 297–312.

Putirka, K.D., 2008. Thermometers and barometers for volcanic systems. In: Putirka, K.D., Tepley, F.J. (Eds.), Minerals, Inclusions, and Volcanic Processes. Reviews in Mineralogy & Geochemistry, vol. 69, pp. 61–120.

Reyes, J., Villaseca, C., Barbero, L., Quejido, A.J., Santos, J.F., 1997. Descripción de un método de separación de Rb, Sr, Sm y Nd en rocas silicatadas para estudios isotópicos. Congreso Ibérico de Geoquímica I 46–55 (in Spanish).

Rudnick, R.L., Gao, S., 2003. Composition of the continental crust. In: Holland, H.D., Turekian, K.K. (Eds.), Treatise on Geochemistry 3. The Crust. Elsevier–Pergamon, Oxford, pp. 1–64.

Scarrow, J.H., Bea, F., Montero, P., Molina, J.F., Vaughan, A.P.M., 2006. A precise late Permian ^{40}Ar/^{39}Ar age for Central Iberian camptonitic lamprophyres. Geol. Acta 4, 451–459.

Scarrow, J.H., Molina, J.F., Bea, F., Montero, P., 2009. Within-plate calc-alkaline rocks: insights from alkaline mafic magma–peraluminous crustal melt hybrid appinites of the Central Iberian Variscan continental collision. Lithos 110, 50–64.

Scarrow, J.H., Molina, J.F., Bea, F., Montero, P., Vaughan, A.P.M., 2011. Lamprophyre dikes as tectonic markers of late orogenic transtension timing and kinematics: a case study from the Central Iberian Zone. Tectonics 30, TC4007.

Scherer, E.E., Münker, C., Mezger, K., 2001. Calibration of the lutetium–hafnium clock. Science 293, 683–687.

Stern, R.J., 2002. Crustal evolution in the East African Orogen: a neodymium isotopic perspective. J. Afr. Earth Sci. 34, 109–117.

Sun, S.S., McDonough, W.F., 1989. Chemical and isotopic systematics of oceanic basalts; implications for mantle composition and processes. In: Saunders, A.D., Norrey, M.J. (Eds.), Magmatism in Ocean Basins, vol. 42. Geological Society of London Special Publication, pp. 313–345.

Sun, J.-F., Yang, J.-H., Wu, F.-Y., Li, X.H., Yang, Y.-H., Xie, L.-W., Wilde, S.A., 2010. Magma mixing controlling the origin of the Early Cretaceous Fangshan granitic pluton, North China Craton: in situ U–Pb age and Sr-, Nd-, Hf- and O-isotope evidence. Lithos 120, 421–438.

Tang, M., Wang, X.-L., Shu, X.-J., Wang, D., Yang, T., Gopon, P., 2014. Hafnium isotopic heterogeneity in zircons from granitic rocks: geochemical evaluation and modeling of "zircon effect" in crustal anatexis. Earth Planet. Sci. Lett. 389, 188–199.

Tappe, S., Foley, S.F., Stracke, A., Romer, R.L., Kjarsgaard, B.A., Heaman, L.M., Joyce, N., 2007. Craton reactivation on the Labrador Sea margins: ^{40}Ar/^{39}Ar age and Sr-Nd-Hf-Pb isotope constraints from alkaline and carbonatite intrusives. Earth Planet. Sci. Lett. 256, 433–454.

Tappe, S., Pearson, D.G., Kjarsgaard, B.A., Nowell, G., Dowall, D., 2013. Mantle transition zone input to kimberlite magmatism near a subduction zone: origin of anomalous Nd–Hf isotope systematics at Lac deGras, Canada. Earth Planet. Sci. Lett. 371–372, 235–251.

Tappe, S., Pearson, D.G., Nowell, G., Nielsen, R.L., Milstead, P., Muehlenbachs, K., 2011. A fresh isotopic look at Greenland kimberlites: cratonic mantle lithosphere imprint on deep source signal. Earth Planet. Sci. Lett. 305, 235–248.

Tappe, S., Smart, K.A., Stracke, A., Romer, R.L., Prelevic, D., van den Bogaard, P., 2016. Melt evolution beneath a rifted craton edge: ^{40}Ar/^{39}Ar geochronology and Sr-Nd-Hf-Pb isotope systematics of primitive alkaline basalts and lamprophyres from the SW Baltic Shield. Geochem. Cosmochim. Acta 173, 1–36.

Turner, S., Arnaud, N., Liu, J., Rogers, N., Hawkesworth, C., Harris, N., Kelley, S., VanCalsteren, P., Deng, W., 1996. Post-collision, shoshonitic volcanism on the Tibetan Plateau: implications for convective thinning of the lithosphere and the source of ocean island basalts. J. Petrol. 37, 45–71.

Ubanell, A.G., Doblas, M., 1987. Los diques aplíticos deformados de Paredes de Escalona–Navamorcuende (SW del Sistema Central Español): su relación con la intrusión. In: Bea, F. (Ed.), Geología de los granitoides y rocas asociadas del Macizo Hespérico. Rueda, Madrid, pp. 393–403 (in Spanish).

Vervoort, J.D., Blichert–Toft, J., 1999. Evolution of the depleted mantle: Hf isotope evidence from juvenile rocks through time. Geochem. Cosmochim. Acta 63, 533–556.

Vilá, M., Pin, C., Enrique, P., Liesa, M., 2005. Telescoping of three distinct magmatic suites in an orogenic setting: generation of Hercynian igneous rocks of the Albera Massif (Eastern Pyrenees). Lithos 83, 97–127.

Villaseca, C., Ancochea, E., Orejana, D., Jeffries, T.E., 2010. Composition and evolution of the lithospheric mantle in central Spain: inferences from peridotite xenoliths from the Cenozoic Calatrava volcanic field. In: Coltorti, M., Downes, H., Grégoire, M., O'Reilly, S.Y. (Eds.), Petrological Evolution of the European Lithospheric Mantle, vol. 337. Geological Society of London Special Publication, pp. 125–151.

Villaseca, C., Barbero, L., Rogers, G., 1998. Crustal origin of Hercynian peraluminous granitic batholiths of central Spain: petrological, geochemical and isotopic (Sr,Nd) arguments. Lithos 43, 55–79.

Villaseca, C., Castiñeiras, P., Orejana, D., 2015. Early Ordovician metabasites from the Spanish central system: a remnant of intraplate HP rocks in the central Iberian zone. Gondwana Res. 27, 392–409.

Villaseca, C., Merino Martínez, E., Orejana, D., Andersen, T., Belousova, E.A., 2016. Zircon Hf signatures from granitic orthogneisses of the Spanish Central System: Significance and sources of the Cambro-Ordovician magmatism in the Iberian Variscan Belt. Gondwana Res. 34, 60–83.

Villaseca, C., Orejana, D., Belousova, E.A., Armstrong, R.A., Pérez–Soba, C., Jeffries, T.E., 2011. U–Pb isotopic ages and Hf isotope composition of zircons in Variscan gabbros from central Spain: evidence of variable crustal contamination. Mineral. Petrol. 101, 151–167.

Villaseca, C., Orejana, D., Pin, C., López García, J.A., Andonaegui, P., 2004. Hercynian and post-Hercynian basic rocks from the Spanish Central System: estimates of Central Spain subcontinental mantle. C. R. Geoscience 336, 877–888.

Wiedenbeck, M., Alle, P., Corfu, F., Griffin, W.L., Meier, M., Oberli, F., Von Quadt, A., Roddick, J.C., Spiegel, W., 1995. Three natural zircon standards for U–Th–Pb, Lu–Hf, trace element and REE analyses. Geostand. Newsl. 19, 1–23.

Wijbrans, J.R., Pringle, M.S., Koppers, A.A.P., Scheveers, R., 1995. Argon geochronology of small samples using the Vulkaan argon laserprobe. Proc. Koninklijke Nederl. Akademie Wetenschappen 98, 185–218.

Wilson, M., 1989. Igneous petrogenesis: a global tectonic approach. Unwin Hyman, Boston, p. 466.

Woodhead D., J., Hergt M., J., 2005. A preliminary appraisal of seven natural zircon reference materials for In situ Hf isotope determination. Geostandards and Geoanalytical Research 29, 183–195.

Yang, J.-H., Sun, J.-F., Chen, F., Wilde, S.A., Wu, F.-Y., 2007. Sources and petrogenesis of late Triassic dolerite dikes in the Liaodong Peninsula: implications for post-collisional lithosphere thinning of the eastern North China Craton. J. Petrol. 48, 1973–1997.

Zeck, H.P., Wingate, M.T.D., Pooley, G., 2007. Ion microprobe U–Pb zircon geochronology of a late tectonic granitic–gabbroic rock complex within the Hercynian Iberian belt. Geol. Mag. 144, 157–177.

Zhang, J., Zhao, Z.-F., Zheng, Y.-F., Liu, X., Xie, L., 2012. Zircon Hf–O isotope and whole-rock geochemical constraints on origin of postcollisional mafic to felsic dykes in the Sulu orogen. Lithos 136–139, 225–245.

Zhao, Z., Mo, X., Dilek, Y., Niu, Y., DePaolo, D.J., Robinson, P., Zhu, D.C., G, S.C., Dong, G.C., Zhou, S., Luo, Z.H., Hou, Z.Q., 2009. Geochemical and Sr–Nd–Pb–O isotopic compositions of the post-collisional ultrapotassic magmatism in SW Tibet: petrogenesis and implications for India intra-continental subduction beneath southern Tibet. Lithos 113, 190–212.